Mechanisms of dissolved and labile particulate iron supply to shelf waters and phytoplankton blooms off South Georgia, Southern Ocean

Christian Schlosser[1,2,*], Katrin Schmidt[3,4], Alfred Aquilina[1], William B. Homoky[1,5], Maxi Castrillejo[1,6], Rachel A. Mills[1], Matthew D. Patey[1], Sophie Fielding[3], Angus Atkinson[7], and Eric P. Achterberg[1,2]

[1] Ocean and Earth Science, National Oceanography Centre Southampton, University of Southampton, SO14 3ZH Southampton, United Kingdom

[2] GEOMAR Helmholtz Centre for Ocean Research, Wischhofstr. 1-3, 24148 Kiel, Germany

[3] British Antarctic Survey, CB3 0ET Cambridge, United Kingdom

[4] School of Geography, Earth and Environmental Sciences, University of Plymouth, PL4 8AA Plymouth, United Kingdom

[5] Department of Earth Sciences, University of Oxford, OX1 3AN Oxford, United Kingdom

[6] Institut de Ciència i Tecnologia Ambientals & Departament de Física, Universitat Autònoma de Barcelona, 08193 Bellaterra, Spain

[7] Plymouth Marine Laboratory, Prospect Place, The Hoe, PL1 3DH Plymouth, United Kingdom

For submission to Biogeosciences

* Corresponding author Christian Schlosser (Email: cschlosser@geomar.de, Phone: 0049 (0) 431 600 1297)

Abstract (369 words)

The island of South Georgia is situated in the iron (Fe) depleted Antarctic Circumpolar Current of the Southern Ocean. Iron emanating from its shelf system fuels large phytoplankton blooms downstream of the island, but the actual supply mechanisms are unclear. To address this, we present an inventory of Fe, manganese (Mn) and aluminium (Al) in shelf sediments, pore waters and the water column in the vicinity of South Georgia, alongside data on zooplankton-mediated Fe cycling processes, and provide estimates of the relative dissolved Fe (DFe) fluxes from these sources. The seafloor sediments were the main particulate Fe source to shelf bottom waters as indicated by the similar Fe/Mn and Fe/Al ratios for shelf sediments and suspended particles in the water column. Less than 1% of the total particulate Fe pool was leachable surface adsorbed (labile) Fe, and therefore potentially available to organisms. Pore waters formed the primary DFe source to shelf bottom waters supplying 0.1 – 44 μmol DFe m^{-2} d^{-1}. However, we estimate that only 0.41 ± 0.26 μmol DFe m^{-2} d^{-1} was transferred to the surface mixed layer by vertical diffusive and advective mixing. Other trace metal sources to surface waters included glacial flour released by melting glaciers and via zooplankton egestion and excretion processes. On average 6.5 ± 8.2 μmol m^{-2} d^{-1} of labile particulate Fe was supplied to the surface mixed layer via faecal pellets formed by Antarctic krill (*Euphausia superba*), with a further 1.1 ± 2.2 μmol DFe m^{-2} d^{-1} released directly by the krill. The faecal pellets released by krill included seafloor-derived lithogenic material and settled algal debris, in addition to freshly ingested suspended phytoplankton cells.

The Fe requirement of the phytoplankton blooms ~1,250 km downstream of South Georgia was estimated at 0.33 ± 0.11 μmol m^{-2} d^{-1}, with the DFe supply by horizontal/vertical mixing, deep winter mixing and aeolian dust estimated as ~0.12 μmol m^{-2} d^{-1}. We hypothesize that a substantial contribution of DFe was provided through recycling of

biogenically stored Fe following luxury Fe uptake by phytoplankton on the Fe-rich shelf. This process would allow Fe to be retained in the surface mixed layer of waters downstream of South Georgia through continuous recycling and biological uptake, supplying the large downstream phytoplankton blooms.

1. Introduction

The Southern Ocean is the largest 'High Nitrate Low Chlorophyll' (HNLC) region of the global ocean (Buesseler et al., 2004), as a consequence of low iron (Fe) supply and subsequent reduced phytoplankton growth (Buesseler et al., 2004; Tsuda et al., 2009). Iron can be supplied to surface waters of the Southern Ocean by atmospheric dust inputs (Cassar et al., 2007; Gao et al., 2001), horizontal/vertical advective and diffusive mixing processes (de Jong et al., 2012), resuspension from shelf sediments (Kalnejais et al., 2010; Marsay et al., 2014), melting of icebergs and glaciers (Raiswell et al., 2008), and hydrothermal inputs (German et al., 2016). Despite the overall HNLC status of the Southern Ocean, regions in the wake of islands feature large seasonal phytoplankton blooms; the Fe sources to these blooms are however poorly constrained (de Jong et al., 2012; Planquette et al., 2007; Pollard et al., 2009).

Downstream of the island of South Georgia intense, long-lasting phytoplankton blooms have been observed which extend hundreds of kilometres, and require an enhanced Fe supply. The blooms peak in austral summer (Borrione et al., 2013), stretch over an area of ~ 750,000 km^2 (Atkinson et al., 2001; Korb et al., 2004), and are responsible for the largest dissolved inorganic carbon deficit reported within the Antarctic Circumpolar Current (ACC) (Jones et al., 2015; Jones et al., 2012). As a consequence of the Fe fertilisation, the waters in the vicinity of South Georgia support extensive phytoplankton blooms and a large biomass of zooplankton, fish, seabirds and marine mammals, some of which are exploited commercially (Atkinson et al., 2001; Murphy et al., 2007).

South Georgia forms part of the volcanically active Scotia Arc in the Atlantic sector of the Southern Ocean and is surrounded by a broad 30 to 100 km wide shelf with an average (albeit highly variable) depth of ca. 200 m (Fig. 1). The island is situated between the Antarctic Polar Front (PF) and the Southern ACC Front (SACCF), within the general

northeast flow of the ACC (Meredith et al., 2005; Whitehouse et al., 2008). The ACC surface waters are enriched in nitrate, phosphate and silicic acid, but strongly depleted in most trace elements, notably Fe and manganese (Mn) (Browning et al., 2014). The large seasonal phytoplankton blooms downstream of South Georgia are thought to be supplied with Fe from the island during the passage of ACC waters (Borrione et al., 2013; Nielsdóttir et al., 2012).

In this study we provide the first comprehensive data set of dissolved and (labile) particulate Fe, Mn, and Al in sediments, pore waters, and the water column overlaying the shelf and shelf edge regions of South Georgia. We also include published data on the role of Antarctic krill in new Fe supply and recycling in this region (Schmidt et al., 2011; Schmidt et al., 2016). We discuss differences between the various analysed trace metal fractions and the supply routes of dissolved and (labile) particulate Fe, such as sedimentary pore water efflux, supply of sediment derived particulate Fe to the surface mixed layer, efflux of Fe from glacial melting and supply of Fe by faecal pellets of Antarctic krill. Furthermore, we discuss the productivity of the bloom region to the north of South Georgia in relation to the estimated Fe supply rates.

2. Methods

2.1 Cruises and Sampling

Samples were collected during three research cruises to South Georgia in 2011 (JR247, JC055), and 2013 (JR274). While cruises JR247 and JR274 aimed to examine the pelagic shelf ecosystem by collection of predominantly water samples (and zooplankton during JR247) on the northern shelf, JC055 explored solely the composition of sediments on the South Georgia shelf. Cruise JR247 took place in January 2011 on RRS *James Clark Ross*, and 14 sites on the northern shelf and shelf edge of South Georgia were visited (stations

1 – 21; Fig. 1). Suspended particles were collected on acid cleaned polycarbonate filters (1 µm pore size; Whatman) using in-situ Stand-Alone Pumping Systems (SAPS; Challenger Oceanic) attached to a Kevlar wire and deployed at 20 m, 50 m and 150 m depth (Fig. 1, red dots). The filters were rinsed with deionized water (Milli-Q; Millipore), stored at -20°C, and shipped frozen to the National Oceanography Centre Southampton (NOCS).

Subsurface seawater samples were collected by trace metal clean samplers (Ocean Test Equipment (OTE)) at 9 of the 14 SAPS locations (Fig. 1; black stars). Seawater samples were filtered using cartridge filter (0.2 µm Sartobran P300; Sartorius) into acid cleaned 125 mL low-density polyethylene (LDPE) bottles (Nalgene). Unfiltered samples were collected in 125 mL LDPE bottles for analysis of total dissolvable (TD) trace metals. Surface waters from the South Georgia shelf were collected using a tow fish deployed alongside the ship at 3 – 4 m depth. Samples were filtered in-line using a cartridge filter (0.2 µm Sartobran P300; Sartorius) and dispensed in acid washed 125 mL LDPE bottles. Unfiltered surface seawater samples were collected and dispensed in acid washed 125 mL LDPE bottles. All seawater samples were acidified on-board with ultra clean HNO_3 (15 M UpA grade, Romil) to pH 1.7 (22 µmol H^+ L^{-1}). For a more detailed description of all sample-handling procedures, please see Supplementary Text S1.

In January and February 2013, RRS *James Clark Ross* cruise JR274 revisited South Georgia and collected surface seawater samples covering the shelf, shelf-edge, and open ocean areas around the island. Dissolved and TD trace elements in surface seawater samples were collected using the tow fish and treated similarly to samples from JR247. For a more detailed description of all sample-handling procedures, please see Supplementary Text S1.

During the RRS *James Cook* cruise JC055 in February 2011, a megacorer (Bowers and Connelly type) was used to collect surface sediment and pore water samples on the southern side of South Georgia (there was no opportunity to sample the northern side of the

island). Cores representing the intact sediment – water interface were retrieved from three sites on the southern shelf, at water depths of ca. 250 m (S1 – S3) (Fig. 1, blue hexagons). Pore waters were separated by centrifugation under N_2 atmosphere and filtered using cellulose nitrate syringe filters (0.2 µm pore size; Whatman (Homoky et al., 2012). Conjugate sediments were freeze dried on board and stored at room temperature. A more detailed description of sediment and pore water sample-handling procedures is provided in Supplementary Text S2.

Krill faecal pellets were obtained during on-board krill incubations performed during JR247. Incubations were performed in darkness in the laminar flow cabinet at ambient surface layer temperature. The krill were incubated in filtered seawater from the tow fish for up to ~3 h immediately after capture, so that pellets obtained derived from material ingested in situ. These incubations and their results are described in more detail in Schmidt et al. (2016).

2.2 Trace metal analysis in suspended particles and krill faecal pellets

The labile trace metal fraction of suspended particles (SAPS) and krill faecal pellets, was remobilized using a 25% acetic acid solution (glacial SpA, Romil) following Planquette et al. (2011). The labile trace metal fraction is hereafter referred to as the leachable particulate trace metal fraction (LP). The remaining particles were digested on a hot plate applying a mixture of aqua regia and hydrogen fluoride (Planquette et al., 2011). This fraction will be referred to as the refractory particulate fraction (RP). The particulate trace metal fraction (P) is the sum of leachable particulate (LP) and refractory particulate (RP). All samples were analysed by collision cell inductively coupled plasma - mass spectrometry (ICP-MS) (ThermoFisher Scientific, XSeriesII). For more detailed description of measured certified reference material see Supplementary Text S1.

2.3 Trace metal analysis of seawater

The filtered and unfiltered seawater samples were stored for a period of 12 months prior to analysis. Concentrations of dissolved and total dissolvable Fe, Mn, and Al in seawater were determined by off-line pre-concentration and isotope dilution / standard addition ICP-MS (ThermoFisher Scientific Element2 XR) according to Rapp et al. (2017). For a more detailed description of the method and measured reference materials see Supplementary Text S1.

2.4 Trace metal analysis of pore waters and sediments

Sub-samples of the bulk, homogenized sediments were fully dissolved following an aqua regia and combined hydrofluoric/perchloric acid digestion method following Homoky et al. (2011). The acid digests and pore waters were analysed by ICP-optical emission spectrometry (OES) (Perkin Elmer Optima 4300DV). For a more detailed description of the method and measured reference materials see Supplementary Text S2.

3. Results & Discussion

3.1 Supply routes of suspended particulate Fe, Mn, and Al

3.1.1 Characterization of (the two) particulate trace metal fractions

Two different particulate fractions were obtained from samples collected during JR247; a particulate fraction from suspended particles collected using 1 µm pore size SAPS filters (P) and a leachable particulate fraction from unfiltered acidified seawater samples (LP_{Un}) collected at the same depth. LP_{Un} was calculated following Eq. (1):

$$LP_{Un} = \text{total dissolvable (TD; unfiltered)} - \text{dissolved (D; 0.2 µm filtered)} \quad (1)$$

Because of the different sampling approaches (SAPS vs. OTE water samplers), filter sizes (>1 µm for SAPS vs. >0.2 µm for dissolved seawater) and digestion procedures (aqua regia + HF for SAPS particles vs. water sample storage at pH 1.7 [22 µmol H^+ L^{-1}]), concentrations of LP_{Un} and P differed, but showed similar distribution patterns in the water column (Fig. 2, Table 1 and 2). The concentrations of Fe, Mn and Al in the LP_{Un} fraction ($LP_{Un}Fe$, $LP_{Un}Mn$, $LP_{Un}Al$) were slightly lower than the particulate fraction from suspended particles (PFe, PMn, PAl). The LP_{Un} of unfiltered seawater samples corresponded to ~ 63 ± 4 % of the PFe, 83 ± 11% of the PAl and 100 ± 10% of the PMn fractions obtained by SAPS. The average LP_{Un} trace metal ratios ($LP_{Un}Fe$/ $LP_{Un}Mn$ = 33.07 ± 3.45 (1 σ) and $LP_{Un}Fe$/ $LP_{Un}Al$ = 0.65 ± 0.10 (n=69)), were about half of the elemental ratios of suspended particles obtained by SAPS (PFe/PMn = 68.0 ± 0.6 and PFe/PAl = 1.251 ± 0.042 (n=42) (Fig. 3; Table 1 and 2)).

The lower concentrations of Fe and Al and the reduced elemental ratios in the LP_{Un} compared to the P fractions suggests that an unknown fraction of particulate Fe and Al in seawater was not leached during the acidification procedure at pH 1.7 over 12 months. However, since P and LP_{Un} displayed similar trends with depth (Fig. 2), LP_{Un} was used in sections 3.1.3 and 3.3 as an indicator for the abundance of particulate trace metals at locations where particulate samples could not be retrieved by SAPS, e.g. in surface waters collected by the tow fish and depths greater than 150 m.

3.1.2 Suspended particulate trace metals in the water column

Concentrations of PFe, PMn and PAl in the water column ranged from 0.87 – 267 nmol L^{-1}, 0.01 – 3.85 nmol L^{-1}, and 0.60 – 195 nmol L^{-1}, respectively (Fig. 2, Table 2). Concentrations of $LP_{Un}Fe$, $LP_{Un}Mn$ and $LP_{Un}Al$ ranged from 1 – 118 nmol L^{-1}, 0.01 – 100 nmol L^{-1}, and 1 – 141 nmol L^{-1}, respectively (Fig. 2, Table 1). Below the isopycnal density layer 27.05 kg m^{-3}, located at ~50 – 70 m depth, P and LP_{Un} increased with depth and showed

a maximum near the seafloor of e.g. 207 nmol L^{-1} for PFe and 112 nmol L^{-1} for $LP_{Un}Fe$ (#17, Table 2). Most sites on the shelf (bottom depth ≤ 260 m; #9/10, #13, #14, #17, and #21) showed seafloor maxima, in agreement with other shelf studies. For example, Milne et al. (2017) reported concentrations of up to 140 nmol L^{-1} for PFe and 800 nmol L^{-1} for PAl in bottom waters on the west African shelf, and Chase et al. (2005) showed bottom water maxima of up to 400 nmol L^{-1} for $LP_{Un}Fe$ off the Oregon coast.

Strong linear relationships between elements were observed for suspended particles (SAPS) obtained from above and below the 27.05 kg m^{-3} isopycnal, with elemental ratios of PFe/PMn = 68.0 ± 0.6 and PFe/PAl = 1.25 ± 0.04 (n=42) (Fig. 3, Table 2). These elemental ratios were higher than those reported for the earth's crust (Fe/Mn = 58, Fe/Al = 0.2, Fe/Ti (titanium) = 9.1 (Wedepohl, 1995)) and sediment samples collected to the south of the island (mean sediment surface layer of S1, S2, S3; SFe/SMn = 51.5 ± 2.4, SFe/SAl = 0.34 ± 0.02 (Fig. 4, Table 3), and SFe/STi = 9.9 (not shown)), suggesting that the suspended particles were more enriched in Fe than lithogenic particles. We are aware that other trace metals, such as Ti, would be more appropriate than Mn to indicate the lithogenic origin of suspended particles. However, the element Ti was not monitored for dissolved, unfiltered seawater and particulate samples obtained by SAPS.

The Fe/Mn ratios among different phytoplankton species show strong variations but are typically much lower (Fe/Mn ~ 1.7 (Ho et al., 2003)), with also lower Fe concentrations than terrestrial/sediment particles (cellular concentration of phytoplankton ~ 0.7 mmol kg^{-1} (Ho et al., 2003); upper crust ~ 550 mmol kg^{-1} (Wedepohl, 1995)). A prevalence of biogenic particles in the suspended particle pool would be expected to result in reduced PFe/PMn ratios in our SAPS samples to values less than 51.5 as was observed in the sediments.

It is most likely that scavenging of DFe onto suspended lithogenic/sediment particles increased the Fe to Al (and Fe to Mn) ratio of suspended particles (PFe/PAl = 1.25; PFe/PMn

= 68.0) compared to sediment particles (SFe/SAl = 0.34; SFe/SMn = 51.5). At seawater pH (~pH 8), dissolved Fe(III) is rapidly hydrolysed to soluble $Fe(III)(OH)_3$ (< 0.02 µm) which readily accumulates as nanometer sized colloids (0.02 – 0.2 µm) (Liu and Millero, 2002). It has been shown that both soluble and colloidal Fe are attracted by charged surfaces, a process that removes DFe and simultaneously increases the amount of particulate Fe in seawater over time (Schlosser et al., 2011).

A range of mechanisms delivers suspended particles to the surface waters. These transport mechanisms will be discussed in the following section.

3.1.3 Glacial outflow and zooplankton feeding activity

While most stations on the shelf showed bottom water maxima of particulate metals, at three sampling sites located on the shelf (#18) and shelf edge (#15/16 and #19/20), the particulate trace metal concentrations featured maxima in the top 100 m of the water column (Fig. 2 and 5). At site #19/20, ca. 100 km away from the coast with a water depth of 1.741 m, the PFe concentration at 20 m depth was 97 nmol L^{-1}, similar to $LP_{Un}Fe$ (Fig. 5). The elemental ratio PFe/PAl of these samples (e.g. 1.01 for site #19/20, 20 m depth) were close to the average ratio (PFe/PAl = 1.25), indicating that lithogenic particles enriched with surface bound Fe dominated the suspended particulate pool in these surface waters.

The surface water maxima of trace metals could have two supply routes: 1) lateral transport of waters containing lithogenic particles from shallow island shelf sediments, and 2) transport of glacial particles following melt processes. The reduced salinities (~33.3) recorded in surface waters in Cumberland Bay and ~50 km offshore of South Georgia (~33.8) (Fig. 6(c) and S1) provide an indication of glacial outflow, melting of icebergs and run-off of melt water streams. Enhanced $LP_{Un}Fe$ concentrations of 2.2 µmol L^{-1} in low salinity surface waters inside Cumberland Bay, are indicative of a meltwater source (LP_{Un} concentration used

as only water samples from the tow fish available). The $LP_{Un}Fe$ concentration decreased strongly with increasing distance from the coast, and exhibited an abrupt reduction to 1 – 5 nmol Fe L^{-1} at the shelf edge ~ 100 km offshore. A similar distribution pattern was observed for $LP_{Un}Mn$ (Fig. 6(d)) and $LP_{Un}Al$ (not shown), for cruises JR247 and JR274. Glacial melt has been reported as an important source of particulate material in the vicinity of the Antarctic Peninsula (de Jong et al., 2012). For example, Gerringa et al. (2012) documented elevated total dissolvable Fe concentration of up to 106 nmol L^{-1} near the Pine Island Glacier in the Amundsen Sea, and Raiswell et al. (2008) estimated that per year 1.6 Gmol nanoparticulate Fe, associated to terrigenous particles, are delivered to the Southern Ocean by melting ice.

Locally elevated particulate metal concentrations in surface waters may also be related to production of faecal pellets by swarms of Antarctic krill (Schmidt et al., 2016). High abundances of Antarctic krill were estimated from acoustic backscattering observations (Fielding et al., 2014), and large numbers of faecal pellets were observed on the SAPS filters during cruise JR247. The stomach content of Antarctic krill contained up to 90% sediment particles by volume, an observation that was attributed to filter feeding by these organisms on phytoplankton and seabed detritus, with incidental ingestion of deep ocean sediments (Schmidt et al., 2011) and glacial flour (Schmidt et al., 2016). Krill thus take up lithogenic particles and transfer these into the surface ocean through the egestion of faecal pellets (Schmidt et al., 2016). The trace metal contents of krill faecal pellets collected during on-board incubation experiments during JR247 ranged from 0.88 – 67.14 µg Fe mg^{-1} dry weight (n = 27) (Table 4) (Schmidt et al. 2016). The molar ratio PFe/PMn = 70.5 ± 8.21 of the faecal pellets was similar to those for suspended particles in the water column (PFe/PMn = 68.0 ± 0.6; Table 1, 2 and 4), indicating that Fe in krill faecal pellets was predominately associated with terrigenous material and/or glacial flour particles, as also reported by Schmidt

et al. (2016). In contrast, the molar ratio PFe/PAl = 0.48 ± 0.07 of faecal pellets was lower than that of suspended particles, PFe/PAl = 1.25 ± 0.04, but higher than that of sediments, PFe/PAl = 0.34 ± 0.02. The observed variability in the PFe/PAl ratio in the various particle pools is therefore a consequence of different contributions of biogenic material to the particulate reservoir and different amounts of Fe scavenged onto particle surfaces.

3.2 Supply routes of dissolved Fe, Mn, and Al

Concentrations of DFe, DMn, and DAl in the water column showed strong variations and ranged from ~ 0.1 – 25.9 nmol L^{-1}, 0.3 – 19.6 nmol L^{-1} and 0.1 – 18.4 nmol L^{-1}, respectively (Fig. 2, 5 and 7), with highest values in the surface waters in Cumberland Bay, and lowest beyond the shelf break (Fig. 6). Dissolved Fe concentrations from this study are in agreement with reported DFe near the Antarctic Peninsula (0.6 – 14.6 nmol L^{-1} (de Jong et al., 2012)) and Crozet Islands (0.1 – 2.5 nmol L^{-1} (Planquette et al., 2007)). Sources and sinks of dissolved trace metals, and their distribution in the water column are discussed in the following sections.

3.2.1 Supply from sediment pore waters

Elevated pore water concentrations of Fe and Mn (Fe_{PW} and Mn_{PW}) were observed in sediments from the southern shelf sites at water depths of around 250 m, and ranged from 0.5 – 110 µmol L^{-1} for Fe and 0.1 – 2 µmol L^{-1} for Mn (Fig. 7 and Table S2). The down-core distributions of Fe_{PW} and Mn_{PW} were consistent with microbial dissimilatory Mn and Fe reduction during organic matter oxidation (Canfield and Thamdrup, 2009), and thus concentrations were elevated at defined depth horizons controlled by their redox potential (Eh) (Bonneville et al., 2009; Raiswell and Canfield, 2012). The Fe_{PW} and Mn_{PW} concentrations near the sediment-seawater interface were used to calculate fluxes of Fe and

Mn to bottom waters following diffusion of reduced Fe and Mn species across an oxygenated layer in surface sediments. These calculations were performed following Boudreau and Scott (1978) and Homoky et al. (2012), and are described in detailed in the Supplementary Text S3 and Table S1. We are aware that our calculated fluxes represent minimum estimates of pore water efflux, which under natural conditions is supplemented by advection due to bioirrigation, bioturbation, and bottom water currents (Homoky et al., 2016). In addition, sediment cores were collected on the southern shelf, while seawater and particulate samples were collected on the northern shelf side. The benthic Fe fluxes for the southern shelf maybe lower than those on the northern shelf, as an elevated primary productivity and enhanced particle export on the northern side will result in enhanced bacterial respiration, which reduces Eh and promotes the dissolution of Fe oxides with subsequent release of Fe into bottom waters.

Notwithstanding the above issues, we calculated substantial benthic fluxes from sediment pore waters to bottom waters on the southern shelf for Fe_{PW} of <0.1 to 44.4 μmol m^{-2} d^{-1} and Mn_{PW} of 0.6 to 4.1 μmol m^{-2} d^{-1}. The upper flux values for Fe are comparable to those reported for dysoxic and river-dominated continental margins (3.5 – 55 μmol m^{-2} d^{-1} (Homoky et al., 2012)), seasonal maxima of temperate and oxic shelf seas (23 – 31 μmol m^{-2} d^{-1} (Klar et al., 2017)), and shelf sediments off the Antarctic Peninsula (1.3 – 15.5 μmol m^{-2} d^{-1} (de Jong et al., 2012)). The Mn fluxes were relatively low for shelf environments, with for example fluxes of 70 – 4450 μmol m^{-2} d^{-1} reported for Baltic and Black Sea sediments (Pakhomova et al., 2007)). The Fe pore water fluxes from the South Georgia shelf sediments, which extend over an area of ca. 40,000 km^2, indicate that these may serve as an important year-round source to overlying waters, totalling 4 to 1,728 kmol DFe d^{-1} and 25 to 164 kmol DMn d^{-1}.

Benthic release of trace metal enriched pore waters shaped the distributions of dissolved trace metals in bottom waters on the shelf. Concentrations of DFe, DMn, and DAl were enhanced at isopycnals > 27.05 kg m^{-3} (e.g. DFe up to 7.70 nmol L^{-1} at site #21, Table 1) compared to surface waters (e.g. DFe as low as 0.30 nmol L^{-1} at site #13, Table 1; Fig. 2 and 7). Trace metal enriched bottom waters were also observed at sites #13, #14, #17 and #18 (Fig. 2). The molar DFe/DMn ratios in oxygenated bottom waters varied between 1.1 – 3.5 and were thus similar to pore waters near the sediment-seawater interface (0 – 1 cm depth, Fe_{PW}/Mn_{PW} = 2.2 ± 1.0; Fig. 7). The similar trace metal ratios suggest that Fe and Mn in enriched pore waters crossed the sediment-bottom water interface and accumulated in shelf bottom waters.

To determine the vertical DFe fluxes from near bottom to surface waters we employed a method outlined by de Jong et al. (2012), and calculated both the advective and diffusive flux terms, which are not affected by the benthic Fe and Mn fluxes. We included the advective term in our calculations, because it has been shown that internal waves that cross shallow topographies and wind shear stress produces strong turbulence that facilitate Eckman upwelling (vertical advection) on the shelf (Kurapov et al., 2010; Moore, 2000; Wolanski and Delesalle, 1995). Applying literature values from the Southern Ocean for vertical diffusivity (K_Z = 1 x 10^{-4} m^2 s^{-1} (Charette et al., 2007)) and advective velocity (w = 1.1 x 10^{-6} m s^{-1} (de Jong et al., 2012)), an average vertical DFe flux on the shelf of 0.41 ± 0.26 µmol m^{-2} d^{-1} from subsurface waters into the surface mixed layer was estimated (Supplementary Text S4). The surface mixed layer depth was determined by a density criteria (~0.03 kg m^{-3} (de Boyer Montégut et al., 2004)) and was located at ~50 m depth. About 38% of the DFe flux was related to Ekman upwelling (advective term) and 62% to the diffusive flux. This vertical flux is at the lower end of the calculated benthic flux from this study (Fe_{PW} < 0.1 to 44.4 µmol m^{-2} d^{-1}), and agrees with values reported for other Southern

Ocean shelf regions near the Antarctic Peninsula (within 20 – 70 km from the coast: ~ 2.7 ± 3.4 µmol m^{-2} d^{-1} (de Jong et al., 2012)) and the Crozet Islands (only diffusive flux of 0.06 µmol m^{-2} d^{-1} (Planquette et al., 2007)).

3.2.2 DFe supply from the leachable particulate fraction

The analytical protocol for the analysis of SAPS-collected particulate material allows separate estimation of the refractory and leachable fractions of trace elements (RP and LP, respectively). The RP fraction of the suspended matter is considered to include silicates and aged oxide minerals, while the LP fraction represents predominantly oxyhydroxides, biogenic material and loosely bound surface associated elements which are readily remobilized using leaching procedures (Berger et al., 2008).

Concentrations of LPFe, LPMn and LPAl in the water column showed strong variations, ranging from a few picomoles to several nanomoles L^{-1} (Table 2). On average, LPFe and LPAl concentrations at 150 m depth (~ 1.3 nmol LPFe L^{-1} and ~0.95 nmol LPAl L^{-1}) were significantly higher than at 20 and 50 m, LPFe = 0.3 nmol L^{-1} (student t-test: t[0.95;28] = 1.725 [1.703]; t[confidence level; n-1]); LPAl = 0.43 nmol L^{-1} (student t-test: t[0.90;28] = 1.383 [1.313]). The LPMn concentrations did not vary strongly and remained near constant throughout the top 150 m (LPMn = 8.9 pmol L^{-1} {student t-test: [0.65;28] = 0.400 [0.390]}). The average contribution of LP to the particulate pool, RP+LP, was low; 0.83 ± 1.13% for Fe, 2.55 ± 1.58% for Mn and 2.42 ± 1.32% for Al (Table 2). A study conducted in the North Pacific near the Columbia River outflow, reported considerably higher LP fractions (e.g. 6.6±3.0% of Fe, 78.7±14.0% of Mn, 6.3±2.0% of Al (Berger et al., 2008)), which was attributed to enhanced biogenic particle levels in the low salinity waters of the river (Berger et al., 2008). In contrast, results from our study showed that particulate

trace metals predominately had a refractory component (RP), indicating that Fe, Mn, and Al was mainly incorporated in lithogenic material.

A weak linear relationship between RP and LP was observed for Fe (R^2 = 0.57, n = 41), Mn (R^2 = 0.64, n = 41) and Al (R^2 = 0.63, n = 41) (Supplementary Fig. S2 and S3), indicating that the LP fraction included mainly Fe, Mn and Al that was scavenged onto lithogenic particle surfaces and not much LPFe was incorporated in biogenic particles. The scavenging of dissolved trace metals by charged particle surfaces is established (Homoky et al., 2012; Koschinsky et al., 2003), but how well Fe and other trace metals can be remobilized from marine particle surfaces and which process may modify their availability over time is not yet well constrained (Achterberg et al., 2018; Fitzsimmons and Boyle, 2014; Milne et al., 2017).

For instance, scavenged Fe is reported to exchange with DFe in the water column of the tropical and high latitude North Atlantic (Achterberg et al., 2018; Fitzsimmons and Boyle, 2014; Milne et al., 2017). In addition, recent work has concluded that zooplankton grazing and the production of faecal pellets remobilizes DFe from lithogenic and biogenic particles (Giering et al., 2012; Schmidt et al., 2016). In contrast, freshly produced inorganic Fe(III) oxyhydroxide ($FeOOH * nH_2O$) precipitates in seawater are subject to chemical and structural conversions that lead to less soluble Fe with time (Yoshida et al., 2006).

3.2.3 DFe supply from Antarctic krill

Elevated dissolved trace metal concentrations in the top 200 m of the water column coincided with elevated particulate trace metal concentrations at sites #11/12, #15/16, #18, and #19/20 (Fig. 2, 5, and 7). The SAPS filters from these stations contained a high load of krill faecal pellets. To elucidate the relationship between dissolved trace metal

concentrations and the local abundance of Antarctic krill and their faecal pellets, krill were caught and incubated on-board the vessel as described in Schmidt et al. (2016).

Antarctic krill excretion rates of DFe were variable, relating positively to the extent of recent ingestion of diatoms. However, on average krill released ~2.0 ± 1.9 nmol DFe individual^{-1} d^{-1} (Schmidt et al., 2016). By applying a mean krill abundance of 465 ± 588 individuals m^{-2}, estimated from acoustic backscattering measurements (Fielding et al., 2014), krill excreted 1.1 ± 2.2 µmol DFe m^{-2} d^{-1} into the top 300 m of the water column (Schmidt et al., 2016). In addition, krill produced ca. 1.8 ± 1.6 mg of faecal pellets per individual per day. Particle leaches performed on those faecal pellet samples with 25% acetic acid showed that on average 2.5 ± 2.1% of the total Fe in these pellets could be remobilised (Table 4), which would equate to a production of 14 ± 24 nmol LPFe ind^{-1} d^{-1}. By multiplying the mean LPFe by the ambient krill density used above, we calculate a LPFe flux of 6.5 ± 8.2 µmol m^{-2} d^{-1} from the faecal pellets to the water column.

Since krill are mobile animals, questions remain over where the major part of the LPFe flux occurs, and what the fate of this Fe source is. Highest krill abundances were recorded generally (but not exclusively) in the top 100 m layer (Fielding et al., 2014), and hence a large proportion of this LPFe flux from krill is likely to occur in the upper waters. Notwithstanding our current uncertainties over the depths of origin and fate, the LPFe flux from krill faecal pellets and the release of DFe were on average an order of magnitude higher than estimated vertical diffusive and advective DFe fluxes, with other grazers, such as copepods and salps, adding to the recycled flux estimates. This illustrates the importance of zooplankton-mediated-Fe-cycling, in agreement with previous studies (Hutchins and Bruland, 1994; Sato et al., 2007).

The experimental set-up did not allow us to establish the origin of the Fe released by krill, being both “recycled” Fe from biogenic material and “new” Fe from lithogenic material.

However, Schmidt et al. (2016) concluded that zooplankton gut passage mobilizes lithogenic Fe, and showed that there are strong spatial patterns in the organic and lithogenic make-up of faecal pellets. This included an exponential decline in the quantity of lithogenic particles in krill stomachs with distance from sources of glacial flour on the northern South Georgia coast. For instance, the lithogenic content at one site on the shelf contributed ~90% of stomach content volume suggesting that a large quantity of the accessible Fe was remobilized from those inorganic particles.

3.3 Off-shore transport of trace metal enriched water masses

Along a W – E transect (Fig. 1; #14 via # 13 to #11/12), lateral water mass transport carried suspended particles offshore. Because of the small size of the SAPS particulate data set (two data points), we considered the LP_{Un} fraction for this transect (Fig. 1). Indeed, elevated concentrations of the P and LP_{Un} metal fractions were observed in subsurface waters that had been in recent contact with the shelf. These metal-enriched waters, detected at the eastern shelf edge site #11/12 between 200 and 400 m water depth (Fig. 1 and 4), exhibited similar temperature and salinity signatures to shelf bottom waters. Furthermore, the elemental ratios of the LP_{Un} fraction in these waters were similar to the particles in the surface sediments (S1, S2, and S3) and the resuspended particles in the bottom boundary layer (#13 and #14) on the shallow shelf (Fig. 4). A similar distribution was also found for the P fractions, but limited to site #13 and #14, as SAPS were not deployed below 150 m at the shelf edge site #11/12.

The $LP_{Un}Fe$ concentration decreased with distance from the island to offshore: from site #14 at 200 m depth ($LP_{Un}Fe$ = 82.26 nmol L^{-1}; water depth = 255 m) to site #13 at 100 m depth ($LP_{Un}Fe$ = 34.06 nmol L^{-1}; water depth = 130 m) to site #11/12 between 200 and 400 m depth ($LP_{Un}Fe$ ~ 10.18 nmol L^{-1}; water depth = 750 m) (Fig.4 and Table 1). A similar

decrease was observed for the SAPS Fe data: from site #14 at 150 m depth (PFe = 31.12 nmol L^{-1}) to site #13 at 100 m depth (PFe = 10.23 nmol L^{-1}). The decrease of PFe and $LP_{Un}Fe$ with increasing distance to the coast is in agreement with previous observations for the Western Subarctic Pacific (Lam and Bishop, 2008), which reported elevated LPFe concentrations in the range of 0.6 to 3.8 nmol L^{-1} in subsurface waters between 100 and 200 m depth along the Kamchatka shelf and related this observation to offshore water mass transport. However, we assume that particles in the deep particulate Fe maximum are not transported over very large distances, due to their tendency to sink, and thus do not significantly contribute to the offshore Fe supply (section 3.4).

Consistent with the observed P and LP_{Un} distributions, elevated dissolved metal concentrations at depths between 200 and 400 m at site #11/12 indicated that trace metal enriched shelf bottom waters were transported offshore (Fig. 7). However, dissolved trace metal concentrations were more variable than P and LP_{Un}, and in case for DMn were highest at depths at shelf edge site #11/12. Notwithstanding the above issue, for horizontal flux calculations we used the entire DFe data set for water depths between 100 and 400 m. Average DFe concentrations in this depth range were highly variable and did not follow an exponential or power law function with distance from the coast (Supplementary Fig. S4), which is necessary to determine scale length and horizontal diffusivity (K_h) (de Jong et al., 2012). As a result, horizontal flux calculations from the data could not be executed.

The distribution of dissolved trace metals in surface waters indicated that there was a limited transfer of DFe beyond the shelf break into the bloom region. Surface samples showed that DFe concentrations were strongly enriched in surface waters on the shelf (0.3 – 25.9 nmol L^{-1}, Fig. 6(b)), while DFe concentrations beyond the shelf break decreased abruptly to concentrations < 0.2 nmol L^{-1} (Fig. 6(b)). This indicates that DFe was quickly removed from ACC surface waters following passage of the island. However, previous

studies in the region suggest DFe transfer beyond the shelf break of South Georgia (Borrione et al., 2013; Nielsdóttir et al., 2012). Nielsdóttir et al. (2012) reported surface waters downstream the island shelf with up to 2 nmol DFe L^{-1}, with seasonal variations and highest concentrations during austral summer in January/February 2008. Dissolved Fe data from JR247 (2011) and JR274 (2012) were also obtained during the summer season, but indicated rapid reduction in concentrations through mixing with DFe depleted ACC water, biological uptake and/or particle scavenging.

3.4 Iron budget in the bloom region

Large seasonal phytoplankton blooms downstream of South Georgia recorded by earth observing satellites are initiated by Fe supplied by the South Georgia island/shelf system during the passage of ACC waters (Fig. 1) (Borrione et al., 2013; Nielsdóttir et al., 2012). Based on our study, the main DFe sources during this passage of the ACC were benthic release and vertical mixing, release of DFe from krill and krill faecal pellets, and supply of particles from run-off and glacial meltwater. In the following sections we will discuss the strength of each DFe source in the bloom region ca. 1,250 km downstream of the island and estimate how much DFe is required to stimulate the elevated primary productivity in that region. Because of the lack of observational data for the region, this part of the study combines literature values from different Southern Ocean studies. This approach contains large uncertainties that are discussed in detail in Section 3.4.6 Budget uncertainties.

3.4.1 Phytoplankton Fe requirements in the phytoplankton bloom region

The surface ocean in the vicinity of South Georgia during the austral summer features strongly elevated biomass production (Gilpin et al., 2002) and represents the largest known CO_2 sink in the ACC (12.9 mmol C m^{-2} d^{-1} (Jones et al., 2012)). The Fe requirements of the

phytoplankton community in austral summer within the bloom that reaches several hundred kilometres downstream the island were determined by combining satellite-depth integrated net primary production data derived from a phytoplankton pigment adsorption (α_{ph})-based model (62 ± 21 mmol C m^{-2} d^{-1} (Ma et al., 2014)) over the period of 2003-2010 with an average intracellular Fe:C ratio obtained from five Southern Ocean diatom species (5.23 ± 2.84 µmol Fe mol^{-1} C (Strzepek et al., 2011)). This approach yielded an approximate Fe requirement of 0.33 ± 0.11 µmol DFe m^{-2} d^{-1} for the phytoplankton community (Fig. 8). For a more detailed description of the applied values and calculations see Supplementary Text S4.

3.4.2 Horizontal and vertical mixing

De Jong et al. (2012) reported that horizontal and vertical advective, diffusive (diapycnal) and deep winter mixing downstream (1,250 – 1,570 km) of the Antarctic Peninsula (between 51°S and 59°S) supplied DFe to the surface waters in quantities that exceeded the DFe requirement of primary producers during austral summer (0.13 ± 0.04 µmol DFe m^{-2} d^{-1}). In their study region, de Jong et al. (2012) determined that ~ 0.30 ± 0.22 µmol DFe m^{-2} d^{-1} were supplied by horizontal and vertical fluxes, of which 91% of the vertical flux were attributed to Ekman upwelling (advective term), and 43% of the entire DFe flux was supplied by deep winter mixing. Tagliabue et al. (2014) reported similar model estimates for the region that is located south of the Polar Front and characterized by strong Ekman upwelling and winter entrainment.

For the bloom region downstream of South Georgia, model calculations by Tagliabue et al. (2014) indicated that less than 0.0003 µmol DFe m^{-2} d^{-1} were supplied by diapycnal mixing, and ~ -0.0027 µmol DFe m^{-2} d^{-1} were removed by Ekman down-welling. For the vertical flux component, this yields an overall loss of DFe of ~ -0.002 µmol DFe m^{-2} d^{-1} (0.0003 + (-0.0027)) in the bloom region north of South Georgia (Fig. 8).

Because the sampling in our study was not suitable for calculations of the horizontal flux, we applied the horizontal flux estimates from de Jong et al. (2012) for our own Fe budget. For a region ca. 1,250 km downstream of a source, calculations according to de Jong et al. (2012) sugest that ca. 0.11 ± 0.03 µmol DFe m^{-2} d^{-1} are supplied to the bloom region by horizontal advection and diffusion (Fig. 8).

3.4.3 Deep winter mixing

The entrainment of new DFe during winter represents an important Fe source to surface waters in the Southern Ocean (de Jong et al., 2012; Tagliabue et al., 2014). Elevated DFe concentrations in subsurface waters support primary production in the austral spring following entrainment by deep winter mixing. Model estimates showed that DFe supplied by winter mixing, together with diapycnal mixing, matches the Fe requirements at most low productivity sites in the Southern Ocean. However, deep winter mixing at the highly productive sites north of South Georgia supplies only ~ 0.011 µmol m^{-2} d^{-1} (Tagliabue et al., 2014) (Fig. 8). Later in the season primary productivity in surface waters is considered to rely strongly on Fe derived from recycling of biogenic material (Boyd et al., 2015).

3.4.4 Dust deposition

Dissolved Fe supplied by the deposition of aeolian dust is considered to be an important source to the Southern Ocean (Conway et al., 2015; Gabric et al., 2010; Gassó and Stein, 2007). Aeolian flux model estimates, supplied by Borrione et al. (2013) using a regional South Georgia model, suggested that up to 8 µmol Fe m^{-2} d^{-1} are delivered to the bloom regions downstream of South Georgia by dry and wet deposition. However, reliable dry and wet deposition estimates for the Southern Ocean are limited. Data from the South Atlantic along 40°S, ~ 1.000 km north of South Georgia, showed that rather low levels of

DFe (~ 0.002 µmol m^{-2} d^{-1}) are supplied by dry deposition (Chance et al., 2015). In addition, ~ 1.0 ± 1.2 µmol DFe m^{-2} d^{-1} are delivered sporadically to the 40°S area by wet deposition (Chance et al., 2015). However, even when assuming that similar wet deposition fluxes occur north of South Georgia, fertilization with DFe is temporally and spatially limited. Furthermore, it is very unlikely that such sporadic events could cause long-lasting and far extending phytoplankton blooms strictly constrained between the PF and the SACCF.

3.4.5 Luxury Fe uptake on the shelf

Our conservative estimate of DFe supply to the bloom region by vertical/horizontal mixing, deep winter entrainment and dust deposition (< 0.12 µmol Fe m^{-2} d^{-1}) covers only ~30% of the estimated phytoplankton requirements (~ 0.33 µmol Fe m^{-2} d^{-1}) (Fig. 8). We hypothesize that the missing supply of ~ 0.21 µmol DFe m^{-2} d^{-1} is supplied to the bloom region through the off-shore advection of phytoplankton cells that are enriched in labile Fe. It has been demonstrated that Fe-rich biogenic particles can be created by luxury iron uptake of diatoms (Iwade et al., 2006; Marchetti et al., 2009). Using bottle incubation experiments, Iwade et al. (2006) showed that under Fe replete conditions the coastal diatom *Chaetoceros sociale* stores more intracellular Fe than needed for the production of essential enzymes and proteins. We therefore hypothesize that phytoplankton cells that grew under excess nutrient supply on the South Georgia shelf stored more Fe than needed for their metabolic processes. Due to subsequent cycles of grazing, lysis or bacterial decomposition, this iron can be remobilised in surface waters and made available for renewed phytoplankton uptake.

High Fe recycling efficiencies, described by the f*e* ratio (Boyd et al., 2005), are required to maintain the cycle of remineralisation and uptake in the euphotic zone. This counteracts the loss of particulate Fe by vertical export. Boyd et al. (2015) reported the highest recycling efficiencies of ~ 90% for subantarctic, DFe-deplete waters such as

downstream of South Georgia. Further, these workers showed that the degree of recycling is controlled by the abundance of prokaryotes with a high Fe quota, such as cyanobacteria, and particularly by grazing zooplankton. The waters off South Georgia feature among the highest biomasses worldwide of metazoan grazers (Atkinson et al., 2001). These large grazers, chiefly copepods and Antarctic krill, are able to efficiently ingest large diatoms including species that are known to store luxury iron (Atkinson, 1994; Hamm et al., 2003), thereby disintegrating cell membranes and releasing trace metals.

In recent years it has become apparent that the recycling of biogenic particles in the euphotic zone is a critical mechanism that maintains primary production, especially when the dissolved nutrient pools become exhausted (Boyd et al., 2015; Tagliabue et al., 2014). However, uncertainties remain over the degree to which Fe is lost during each cycle of uptake and remineralisation. Thus more research is needed, especially field work that encompasses the community structures (bacteria, phytoplankton, zooplankton, and higher predators (Ratnarajah et al., 2017; Wing et al., 2014)), the degree of recycling for macro- and micro-nutrients in the euphotic zone, and loss of Fe through vertical export.

An alternative explanation to our suggestion that recycling of luxury iron enriched biota contributes to the downstream bloom is that iron is adsorbed directly onto particles that are advected directly offshore. For example freshly precipitated Fe(III) oxyhydroxides ($FeOOH * nH_2O$) may be adsorbed onto biogenic and non-biogenic material. Iron freshly absorbed onto biogenic and non-biogenic material can be released and incorporated by phytoplankton and bacteria. However, the bioavailability of adsorbed and inorganic Fe changes over time. Both Wells et al. (1991) and Chen and Wang (2001) demonstrated that the bioavailability of freshly precipitated FeOOH and Fe adsorbed onto colloids/inorganic particles decreases over time. This is primarily due to the dehydration of the loosely packed structure that is subsequently transferred into amorphous FeOOH in the mineral structure

Goethite. Because of this we suggest that the majority of Fe from inorganic FeOOH or Fe adsorbed onto particles must be released and utilized in an early stage of the voyage, mainly on the shelf or shortly after the shelf break.

3.4.6 Budget uncertainties

Estimates for Fe budgets are challenging and often contain large uncertainties. This is primarily due to the lack of site- and time-specific flux data. Moreover, the mean annual estimates, necessary for reliable supply calculations, reach a high level of accuracy only after the same region has been monitored multiple times to cover seasonal and annual anomalies. In the following, we will discuss the uncertainty of the different Fe fluxes in the blooming region north of South Georgia.

We identified three main processes that account together for ~98% of the total Fe flux in the blooming region, and thus contribute largest uncertainties; the horizontal flux, dry/wet deposition, and winter entrainment. Horizontal flux estimates of this study rely on literature values that were collected offshore the Antarctic Peninsula. In contrast, South Georgia is an island with a confined shelf region and thus horizontal DFe fluxes may differ greatly. Furthermore, we showed that dry deposition dust fluxes are generally low, but showed in addition that the Fe flux can be supplemented strongly by sporadic wet deposition events (~ 1.0 ± 1.2 µmol DFe m^{-2} d^{-1}) (Chance et al., 2015). Atmospheric fluxes are variable, illustrated by the large standard deviation of the wet deposition Fe fluxes obtained at 40°S. Furthermore, to determine the magnitude of the seasonal DFe winter entrainment reliable estimates of the winter mixing layer depth (WMLD) and the ferrocline are required. Even though the WMLD can be estimated very precisely using Argo float data, the depth of ferrocline in the manuscript of Tagliabue et al. (2014) is based on 140 unique observations distributed over the entire Southern Ocean. Due to this regional anomalies are not captured.

In addition to the DFe fluxes in the blooming region, we also assume that the biological Fe demand estimated for the phytoplankton community contributes a large error. The biological Fe requirements were determined using satellite derived net primary production data and an average intracellular Fe:C ratio derived from 5 different diatom species native to the Southern Ocean. Both parameters are not well constrained and because of the lack of observational data we applied the lowest intracellular Fe:C ratio available in the literature (Strzepek et al., 2011). However, we found that even small changes of the both parameters change the estimated Fe availability in the bloom region strongly. Nevertheless, flux estimates even with large uncertainties can help us understand the degree of the nutrient supply vs. consumption by organisms and help to pinpoint the limitation of the estimates made. To ultimately reduce the level of uncertainty and to improve our biogeochemical models more observational data from the bloom region north of South Georgia is required.

4. Conclusions

Shelf sediment-derived Fe and Fe released from Antarctic krill significantly contribute to the DFe distribution in the shelf waters around South Georgia. Nevertheless, DFe enriched in shelf waters are not effectively advected to the phytoplankton bloom region downstream of the island. Together with other Fe supplies, such as aeolian dust, deep winter mixing and diapycnal mixing, the horizontal advection contributes only ~30% to the Fe requirements of a phytoplankton bloom downstream of South Georgia. We therefore hypothesize that the majority of the Fe is derived from remineralisation of Fe enriched phytoplankton cells and biogenic particles that are transported with the water masses into the bloom region.

While we highlight the importance of grazers and the cycling of various particulate Fe phases in the Fe-fertilisation of the South Georgia bloom, more work is needed to clarify the transport mechanisms of dissolved and particulate Fe.

Author contribution

CS, KS, EPA, SF, and AAt designed the experiments for JC247. CS, MDP and AAt performed the sampling and krill incubation experiments during JC247. CS and MC analysed the trace metal samples at NOCS. EPA sampled the seawater during JC274. Samples from JC274 were analysed by CS and MC. AAq, WBH and RM designed the experiments for JR55 and AAq analysed the samples. CS prepared the manuscript with contributions from all co-authors.

Acknowledgements

We would like to thank the officers and crew of RRS *James Clark Ross* for assistance with the pelagic sampling and those of RRS *James Cook* for the benthic coring. In addition, we thank the two anonymous reviewers for reviewing the manuscript. This work forms part of the NERC-AFI grant AFI9/07 to AA and EA (NE/F01547X/1). RAM was funded by NERC grants NE/01249X/1 and NE/H004394/1. WBH was supported by NERC fellowship NE/K009532/1

References

Achterberg, E. P., Steigenberger, S., Marsay, C. M., LeMoigne, F. A. C., Painter, S. C., Baker, A. R., Connelly, D. P., Moore, C. M., Tagliabue, A., and Tanhua, T.: Iron Biogeochemistry in the High Latitude North Atlantic Ocean, Scientific Reports, 8, 1283, 2018.

Atkinson, A.: Diets and feeding selectivity among the epipelagic copepod community near South Georgia in summer, Polar Biol., 14, 551-560, 1994.

Atkinson, A., Whitehouse, M. J., Priddle, J., Cripps, G. C., Ward, P., and Brandon, M. A.: South Georgia, Antarctica: a productive, cold water, pelagic ecosystem, Mar. Ecol.-Prog. Ser., 216, 279-308, 2001.

Berger, C. J. M., Lippiatt, S. M., Lawrence, M. G., and Bruland, K. W.: Application of a chemical leach technique for estimating labile particulate aluminum, iron, and manganese in the Columbia River plume and coastal waters off Oregon and Washington, J. Geophys. Res., 113, 1-16, 2008.

Bonneville, S., Behrends, T., and Van Cappellen, P.: Solubility and dissimilatory reduction kinetics of iron(III) oxyhydroxides: A linear free energy relationship, Geochim. Cosmochim. Act., 73, 5273-5282, 2009.

Borrione, I., Aumont, O., Nielsdottir, M. C., and Schlitzer, R.: Sedimentary and atmospheric sources of iron around South Georgia, Southern Ocean: a modelling perspective, Biogeosciences Discuss., 10, 10811-10858, 2013.

Boudreau, B. P. and Scott, M. R.: A model for the diffusion-controlled growth of deep-sea manganese nodules, Americ. J. Sc., 278, 903-929, 1978.

Boyd, P. W., Law, C. S., Hutchins, D. A., Abraham, E. R., Croot, P. L., Ellwood, M., Frew, R. D., Hadfield, M., Hall, J., Handy, S., Hare, C., Higgins, J., Hill, P., Hunter, K. A., LeBlanc, K., Maldonado, M. T., McKay, R. M., Mioni, C., Oliver, M., Pickmere, S.,

Pinkerton, M., Safi, K., Sander, S., Sanudo-Wilhelmy, S. A., Smith, M., Strzepek, R., Tovar-Sanchez, A., and Wilhelm, S. W.: FeCycle: Attempting an iron biogeochemical budget from a mesoscale SF6 tracer experiment in unperturbed low iron waters, Global Biogeochem. Cycles, 19, 1-13, 2005.

Boyd, P. W., Strzepek, R. F., Ellwood, M. J., Hutchins, D. A., Nodder, S. D., Twining, B. S., and Wilhelm, S. W.: Why are biotic iron pools uniform across high- and low-iron pelagic ecosystems?, Global Biogeochem. Cycles, 29, 1028-1043, 2015.

Browning, T. J., Bouman, H. A., Henderson, G. M., Mather, T. A., Pyle, D. M., Schlosser, C., Woodward, E. M. S., and Moore, C. M.: Strong responses of Southern Ocean phytoplankton communities to volcanic ash, Geophys. Res. Lett., 41, 1-7, 2014.

Buesseler, K. O., Andrews, J. E., Pike, S. M., and Charette, M. A.: The Effects of Iron Fertilization on Carbon Sequestration in the Southern Ocean, Science, 304, 414-417, 2004.

Canfield, D. E. and Thamdrup, B.: Towards a consistent classification scheme for geochemical environments, or, why we wish the term ‘suboxic’ would go away, Geobiol., 7, 385-392, 2009.

Cassar, N., Bender, M. L., Barnett, B. A., Fan, S., Moxim, W. J., Levy II, H., and Tilbrook, B.: The Southern Ocean Biological Response to Aelian Iron Input, Science, 317, 1067-1070, 2007.

Chance, R., Jickells, T. D., and Baker, A. R.: Atmospheric trace metal concentrations, solubility and deposition fluxes in remote marine air over the south-east Atlantic, Mar. Chem., 177, 45-55, 2015.

Charette, M. A., Gonneea, M. E., Morris, P., Statham, P., Fones, G., Planquette, H., Salter, I., and Garabato, A. N.: Radium isotopes as tracers of iron sources fueling a Southern Ocean phytoplankton bloom, Deep-Sea Res. II, 54, 1989-1998, 2007.

Chase, Z., Hales, B., Cowles, T., Schwartz, R., and van Geen, A.: Distribution and variability of iron input to Oregon coastal waters during the upwelling season, J. Geophys. Res., 110, 1-14, 2005.

Chen, M. and Wang, W.-X.: Bioavailability of natural colloid-bound iron to marine plankton: Influences of colloidal size and aging, Limnol. Oceanogr., 46, 1956-1967, 2001.

Conway, T. M., Wolff, E. W., Rothlisberger, R., Mulvaney, R., and Elderfield, H. E.: Constraints on soluble aerosol iron flux to the Southern Ocean at the Last Glacial Maximum, Nat. Commun., 6, 1-9, 2015.

de Boyer Montégut, C., Madec, G., Fischer, A. S., Lazar, A., and Iudicone, D.: Mixed layer depth over the global ocean: An examination of profile data and a profile-based climatology, J. Geophys. Res., 109, 1-20, 2004.

de Jong, J., Schoemann, V., Lannuzel, D., Croot, P., de Baar, H. J. W., and Tison, J. L.: Natural iron fertilization of the Atlantic sector of the Southern Ocean by continental shelf sources of the Antarctic Peninsula, J. Geophys. Res., 117, 1-25, 2012.

Fielding, S., Watkins, J. L., Trathan, P. N., Enderlein, P., Waluda, C. M., Stowasser, G., Tarling, G. A., and Murphy, E. J.: Interannual variability in Antarctic krill (Euphausia superba) density at South Georgia, Southern Ocean: 1997–2013, ICES J. Mar. Sci., 2014. 1-11, 2014.

Fitzsimmons, J. N. and Boyle, E. A.: Both soluble and colloidal iron phases control dissolved iron variability in the tropical North Atlantic Ocean, Geochim. Cosmochim. Act., 125, 539-550, 2014.

Gabric, A. J., Cropp, R. A., McTainsh, G. H., Johnston, B. M., Butler, H., Tilbrook, B., and Keywood, M.: Australian dust storms in 2002 and 2003 and their impact on Southern Ocean biogeochemistry, Global Biogeochem. Cycles, 24, 1-17, 2010.

Gao, Y., Kaufman, Y. J., Tanré, D., Kolber, D., and Falkowski, P. G.: Seasonal distributions of aeolian iron fluxes to the global ocean, Geophys. Res. Lett., 28, 29-32, 2001.

Gassó, S. and Stein, A. F.: Does dust from Patagonia reach the sub-Antarctic Atlantic Ocean?, Geophys. Res. Lett., 34, 1-5, 2007.

German, C. R., Casciotti, K. A., Dutay, J.-C., Heimbürger, L. E., Jenkins, W. J., Measures, C. I., Mills, R. A., Obata, H., Schlitzer, R., Tagliabue, A., Turner, D. R., and Whitby, H.: Hydrothermal impacts on trace element and isotope ocean biogeochemistry, Philos Trans A Math Phys Eng Sci, 374, 1-19, 2016.

Gerringa, L. J. A., Alderkamp, A.-C., Laan, P., Thuróczy, C.-E., De Baar, H. J. W., Mills, M. M., van Dijken, G. L., van Haren, H., and Arrigo, K. R.: Iron from melting glaciers fuels the phytoplankton blooms in Amundsen Sea (Southern Ocean): Iron biogeochemistry, Deep-Sea Res. II, 71-76, 16-31, 2012.

Giering, S. L. C., Steigenberger, S., Achterberg, E. P., Sanders, R., and Mayor, D. J.: Elevated iron to nitrogen recycling by mesozooplankton in the Northeast Atlantic Ocean, Geophys. Res. Lett., 39, L12608, 2012.

Gilpin, L. C., Priddle, J., Whitehouse, M. J., Savidge, G., and Atkinson, A.: Primary production and carbon uptake dynamics in the vicinity of South Georgia-balancing carbon fixation and removal, Mar. Ecol. Prog. Ser., 242, 51-62, 2002.

Hamm, C. E., Merkel, R., Springer, O., Jurkojc, P., Maier, C., Prechtel, K., and Smetacek, V.: Architecture and material properties of diatom shells provide effective mechanical protection, Nature, 421, 841-843, 2003.

Ho, T.-Y., Quigg, A., Finkel, Z. V., Milligan, A. J., Wyman, K., Falkowski, P. G., and Morel, F. M. M.: The elemental composition of some marine phytoplankton, J. Phycol., 39, 1145-1159, 2003.

Homoky, W. B., Hembury, D. J., Hepburn, L. E., Mills, R. A., Statham, P. J., Fones, G. R., and Palmer, M. R.: Iron and manganese diagenesis in deep sea volcanogenic sediments and the origins of pore water colloids, Geochim. Cosmochim. Act., 75, 5032-5048, 2011.

Homoky, W. B., Severmann, S., McManus, J., Berelson, W. M., Riedel, T. E., Statham, P. J., and Mills, R. A.: Dissolved oxygen and suspended particles regulate the benthic flux of iron from continental margins, Mar. Chem., 134–135, 59-70, 2012.

Homoky, W. B., Weber, T., Berelson, W. M., Conway, T. M., Henderson, G. M., van Hulten, M., Jeandel, C., Severmann, S., and Tagliabue, A.: Quantifying trace element and isotope fluxes at the ocean–sediment boundary: a review, Philos Trans A Math Phys Eng Sci, 374, 2016.

Hutchins, D. A. and Bruland, K. W.: Grazer-mediated regeneration and assimilation of Fe, Zn and Mn from planktonic prey, Mar. Ecol.-Prog. Ser., 110, 259-269, 1994.

Iwade, S., Kuma, K., Isoda, Y., Yoshida, M., Kudo, I., Nishioka, J., and Suzuki, K.: Effect of high iron concentrations on iron uptake and growth of a coastal diatom Chaetoceros sociale, Aquat. Microb. Ecol., 43, 177-191, 2006.

Jones, E. M., Bakker, D. C. E., Venables, H. J., and Hardman-Mountford, N. J.: Seasonal cycle of CO2 from the sea ice edge to island blooms in the Scotia Sea, Southern Ocean, Mar. Chem., 177, 490-500, 2015.

Jones, E. M., Bakker, D. C. E., Venables, H. J., and Watson, A. J.: Dynamic seasonal cycling of inorganic carbon downstream of South Georgia, Southern Ocean, Deep-Sea Res. II, 59–60, 25-35, 2012.

Kalnejais, L. H., Martin, W. R., and Bothner, M. H.: The release of dissolved nutrients and metals from coastal sediments due to resuspension, Mar. Chem., 121, 224-235, 2010.

Klar, J. K., Homoky, W. B., Statham, P. J., Birchill, A. J., Harris, E. L., Woodward, E. M. S., Silburn, B., Cooper, M. J., James, R. H., Connelly, D. P., Chever, F., Lichtschlag, A., and

Graves, C.: Stability of dissolved and soluble Fe(II) in shelf sediment pore waters and release to an oxic water column, Biogeochemistry, 2017. 1-19, 2017.

Korb, R. E., Whitehouse, M. J., and Ward, P.: SeaWiFS in the southern ocean: spatial and temporal variability in phytoplankton biomass around South Georgia, Deep-Sea Res. II, 51, 99-116, 2004.

Koschinsky, A., Winkler, A., and Fritsche, U.: Importance of different types of marine particles for the scavenging of heavy metals in the deep-sea bottom water, Appl Geochem, 18, 693-710, 2003.

Kurapov, A. L., Allen, J. S., and Egbert, G. D.: Combined Effects of Wind-Driven Upwelling and Internal Tide on the Continental Shelf, Journal of Physical Oceanography, 40, 737-756, 2010.

Lam, P. J. and Bishop, J. K. B.: The continental margin is a key source of iron to the HNLC North Pacific Ocean, Geophys. Res. Lett., 35, 1-5, 2008.

Liu, X. and Millero, F. J.: The solubility of iron in seawater, Mar. Chem., 77, 43-54, 2002.

Ma, S., Tao, Z., Yang, X., Yu, Y., Zhou, X., M, W., and Li, Z.: Estimation of marine primary productivity from satellite-derived phytoplankton absorption data, IEEE J-STARS, 7, 3084-3092, 2014.

Marchetti, A., Parker, M. S., Moccia, L. P., Lin, E. O., Arrieta, A. L., Ribalet, F., Murphy, M. E. P., Maldonado, M. T., and Armbrust, E. V.: Ferritin is used for iron storage in bloom-forming marine pennate diatoms, Nature, 457, 467-470, 2009.

Marsay, C. M., Sedwick, P. N., Dinniman, M. S., Barrett, P. M., Mack, S. L., and McGillicuddy, D. J.: Estimating the benthic efflux of dissolved iron on the Ross Sea continental shelf, Geophys. Res. Lett., 41, 7576-7583, 2014.

Meredith, M. P., Brandon, M. A., Murphy, E. J., Trathan, P. N., Thorpe, S. E., Bone, D. G., Chernyshkov, P. P., and Sushin, V. A.: Variability in hydrographic conditions to the east and northwest of South Georgia, 1996–2001, J. Marine Syst., 53, 143-167, 2005.

Milne, A., Schlosser, C., Wake, B. D., Achterberg, E. P., Chance, R., Baker, A. R., Forryan, A., and Lohan, M. C.: Particulate phases are key in controlling dissolved iron concentrations in the (sub)tropical North Atlantic, Geophys. Res. Lett., 44, 2377-2387, 2017.

Moore, W. S.: Determining coastal mixing rates using radium isotopes, Cont. Shelf Res., 20, 1993-2007, 2000.

Murphy, E. J., Trathan, P. N., Watkins, J. L., Reid, K., Meredith, M. P., Forcada, J., Thorpe, S. E., Johnston, N. M., and Rothery, P.: Climatically driven fluctuations in Southern Ocean ecosystems, P ROY SOC B-BIOL SCI, 274, 3057-3067, 2007.

Nielsdóttir, M. C., Bibby, T. S., Moore, C. M., Hinz, D. J., Sanders, R., Whitehouse, M., Korb, R., and Achterberg, E. P.: Seasonal and spatial dynamics of iron availability in the Scotia Sea, Mar. Chem., 130–131, 62-72, 2012.

Pakhomova, S. V., Hall, P. O. J., Kononets, M. Y., Rozanov, A. G., Tengberg, A., and Vershinin, A. V.: Fluxes of iron and manganese across the sediment–water interface under various redox conditions, Mar. Chem., 107, 319-331, 2007.

Planquette, H., Sanders, R., Statham, P. J., Morris, P. J., and Fones, G. R.: Fluxes of particulate iron from the upper ocean around the Crozet Islands: A naturally iron-fertilized environment in the Southern Ocean, Global Biogeochem. Cycles, 25, 1-12, 2011.

Planquette, H., Statham, P. J., Fones, G. R., Charette, M. A., Moore, C. M., Salter, I., Nedelec, F. H., Taylor, S. L., French, M., Baker, A. R., Mahowald, N., and Jickells, T. D.: Dissolved iron in the vicinity of the Crozet Islands, Southern Ocean, Deep-Sea Res. II, 54, 1999-2019, 2007.

Pollard, R. T., Salter, I., Sanders, R. J., Lucas, M. I., Moore, C. M., Mills, R. A., Statham, P. J., Allen, J. T., Baker, A. R., Bakker, D. C. E., Charette, M. A., Fielding, S., Fones, G. R., French, M., Hickman, A. E., Holland, R. J., Hughes, J. A., Jickells, T. D., Lampitt, R. S., Morris, P. J., Nedelec, F. H., Nielsdottir, M., Planquette, H., Popova, E. E., Poulton, A. J., Read, J. F., Seeyave, S., Smith, T., Stinchcombe, M., Taylor, S., Thomalla, S., Venables, H. J., Williamson, R., and Zubkov, M. V.: Southern Ocean deep-water carbon export enhanced by natural iron fertilization, Nature, 457, 577-580, 2009.

Raiswell, R., Benning, L. G., Tranter, M., and Tulaczyk, S.: Bioavailable iron in the Southern Ocean: the significance of the iceberg conveyor belt, Geochemical Transactions, 9, 1-9, 2008.

Raiswell, R. and Canfield, D. E.: The Iron Biogeochemical Cycle Past and Present, Geochemical Perspectives, 1, 1-2, 2012.

Rapp, I., Schlosser, C., Rusiecka, D., Gledhill, M., and Achterberg, E. P.: Automated preconcentration of Fe, Zn, Cu, Ni, Cd, Pb, Co, and Mn in seawater with analysis using high-resolution sector field inductively-coupled plasma mass spectrometry, Anal. Chimi. Acta, 976, 1-13, 2017.

Ratnarajah, L., Lannuzel, D., Townsend, A. T., Meiners, K. M., Nicol, S., Friedlaender, A. S., and Bowie, A. R.: Physical speciation and solubility of iron from baleen whale faecal material, Mar. Chem., 2017. 2017.

Sato, M., Takeda, S., and Furuya, K.: Iron regeneration and organic iron(III)-binding ligand production during in situ zooplankton grazing experiment, Mar. Chem., 106, 471-488, 2007.

Schlosser, C., De La Rocha, C. L., and Croot, P. L.: Effects of iron surface adsorption and sample handling on iron solubility measurements, Mar. Chem., 127, 48-55, 2011.

Schmidt, K., Atkinson, A., Steigenberger, S., Fielding, S., Lindsay, M. C. M., Pond, D. W., Tarling, G. A., Klevjer, T. A., Allen, C. S., Nicol, S., and Achterberg, E. P.: Seabed foreaging

by Antarctic krill: Implications for stock assessment, bentho-pelagic coupling, and the vertical transfer of iron, Limnol. Oceanogr., 56, 1411-1428, 2011.

Schmidt, K., Schlosser, C., Atkinson, A., Fielding, S., Venables, H. J., Waluda, C. M., and Achterberg, E. P.: Zooplankton gut passage mobilises lithogenic iron for ocean productivity, Curr. Biol., 26, 1-7, 2016.

Strzepek, R., Maldonado, M. T., Hunter, K. A., Frew, R. D., and Boyd, P. W.: Adaptive strategies by Southern Ocean phytoplankton to lessen iron limitation: Uptake of organically complexed iron and reduced cellular iron requirements, Limnol. Oceanogr., 56, 1983-2002, 2011.

Tagliabue, A., Sallee, J.-B., Bowie, A. R., Levy, M., Swart, S., and Boyd, P. W.: Surface-water iron supplies in the Southern Ocean sustained by deep winter mixing, Nat Geosci, 7, 314-320, 2014.

Tsuda, A., Saito, H., Machida, R. J., and Shimode, S.: Meso- and microzooplankton responses to an in situ iron fertilization experiment (SEEDS II) in the northwest subarctic Pacific, Deep-Sea Res. II, 56, 2767-2778, 2009.

Wedepohl, K. H.: The composition of the continental crust, Geochim. Cosmochim. Act., 59, 1217-1232, 1995.

Wells, M. L., Mayer, L. M., Donard, O. F. X., Sierra, M. M. D., and Ackelson, S. G.: The Photolysis Of Colloidal Iron In The Oceans, Nature, 353, 248-250, 1991.

Whitehouse, M. J., Korb, R. E., Atkinson, A., Thorpe, S. E., and Gordon, M.: Formation, transport and decay of an intense phytoplankton bloom within the High-Nutrient Low-Chlorophyll belt of the Southern Ocean, J. Marine Syst., 70, 150-167, 2008.

Wing, S. R., Jack, L., Shatova, O., Leichter, J. J., Barr, D., Frew R. D., and Gault-Ringold, M.: Seabirds and marine mammals redistribute bioavailable iron in the Southern Ocean, Mar. Ecol. Prog. Ser., 510, 1-13, 2014.

Wolanski, E. J. and Delesalle, B.: Upwelling by internal waves, Tahiti, French Polynesia, Cont. Shelf Res., 15, 357-368, 1995.

Yoshida, M., Kuma, K., Iwade, S., Isoda, Y., Takata, H., and Yamada, M.: Effect of aging time on the availability of freshly precipitated ferric hydroxide to costal marine diatoms, Mar. Biol., 149, 379-392, 2006.

Table 1: OTE-seawater samples: Fe, Mn, and Al concentrations determined for the dissolved (D) (0.2 µm) and the leachable particulate fraction (LP_{UN}) (total dissolvable – dissolved) of unfiltered seawater samples collected during JR247. Additional information covers sampling date, site (station) ID, event number and latitude + longitude.

Date	Site ID	Depth	Leach. Part. (nmol L^{-1})			Dissolved (nmol L^{-1})		
	Lat. & Lon.	(m)	$LP_{Un}Fe$	$LP_{Un}Mn$	$LP_{Un}Al$	DFe	DMn	DAl
04/01/2011	#9/10 (E95 & E97)	20	20.36	0.95	46.41	5.71	1.83	1.11
		50	15.18	0.42	40.86	3.19	1.88	2.27
	54.26°S, 35.35°W	100	9.86	0.23	20.43	1.55	0.92	2.07
		130	23.33	0.73	48.91	2.82	0.87	2.68
		150	23.71	0.43	46.95	2.35	1.03	0.12
		200	27.37	0.62	54.41	2.70	0.89	2.37
05/01/2011	#11/12 (E98 & E101)	20	4.05	0.38	6.68	2.19	0.41	3.57
		35	1.52	0.39	7.28	0.41	0.37	-
	54.62°S, 34.81°W	50	9.30	0.60	22.20	7.18	0.64	13.31
		75	1.28	0.31	7.85	0.77	0.35	4.56
		100	2.02	0.32	3.34	1.09	0.35	1.47
		150	1.55	0.38	3.18	1.10	0.45	-
		200	13.10	1.31	23.81	1.26	1.17	3.07
		300	8.62	0.70	23.25	1.06	0.55	-
		400	8.81	0.54	16.54	2.05	0.46	2.69
		500	4.51	0.41	11.41	0.72	0.38	0.76
		600	2.75	0.37	10.32	0.96	0.36	0.77
		700	4.81	0.41	16.85	0.82	0.35	-
06/01/2011	#13 (E105)	20	3.46	0.62	14.68	0.28	0.57	4.53
		35	1.00	0.33	7.17	0.10	0.28	2.64
	54.53°S, 35.27°W	50	7.09	0.71	22.62	1.26	0.57	5.77
		75	25.03	1.09	61.94	1.23	0.64	5.86
		100	34.06	1.30	87.43	0.82	0.74	4.08
07/01/2011	#14 (E113)	20	4.00	0.89	7.87	0.64	0.85	2.57
		50	2.23	0.31	7.64	0.27	0.32	1.80
	54.56°S, 35.59°W	75	2.30	0.43	3.58	0.62	0.46	2.42
		100	2.26	0.44	3.34	0.35	0.46	0.46
		150	23.50	0.94	33.35	0.70	0.62	0.23
		200	82.26	2.12	103.11	2.69	0.77	2.31
08/01/2011	#15/16 (E119 & E129)	20	17.66	0.46	26.66	0.99	1.36	-
		35	16.60	0.30	13.37	0.96	1.27	-
	53.62°S, 36.34°W	50	16.30	0.23	18.49	1.21	1.40	-
		75	23.82	0.56	29.86	0.98	1.28	-
		100	8.49	0.10	10.50	0.73	0.56	-
		150	1.88	0.03	4.49	2.25	0.40	-
		200	2.72	0.02	1.40	0.63	0.44	2.87

		300	2.56	0.05	2.40	0.34	0.25	-
		400	3.75	0.02	5.28	0.48	0.30	1.17
		500	5.28	0.08	9.22	0.43	0.30	-
		600	5.50	0.09	11.45	0.53	0.28	1.63
		750	5.27	0.06	8.16	0.44	0.30	-
10/01/2011	#17 (E133)	20	10.92	0.22	7.43	2.31	1.20	3.76
		35	20.83	0.53	16.22	1.81	1.34	2.56
	53.90°S, 36.57°W	50	34.59	1.00	57.55	2.29	1.42	2.33
		75	118.25	2.18	64.36	4.21	1.86	2.19
		100	50.71	1.00	77.52	2.48	1.42	1.62
		150	112.28	2.23	86.09	3.39	1.41	0.86
11/01/2011	#18 (E138)	20	106.71	1.77	95.17	2.75	1.57	3.36
		35	83.53	0.00	100.32	1.97	1.33	2.44
	54.10°S, 36.25°W	50	9.67	0.00	18.23	0.74	0.85	-
		75	5.65	0.00	8.90	0.62	0.65	-
		100	4.50	0.08	23.65	1.25	0.48	5.18
		150	7.81	0.11	12.87	1.43	0.49	8.19
12/01/2011	#19/20 (E141 & E143)	20	60.19	2.11	54.29	1.46	1.71	5.30
		35	60.17	2.19	87.17	1.34	1.90	8.22
	53.54°S, 38.11°W	50	66.78	2.74	141.75	1.57	1.90	8.73
		75	71.69	1.78	79.19	1.61	2.13	11.45
		100	10.77	0.25	32.12	0.99	0.67	10.74
		150	5.43	0.13	31.35	1.84	0.92	12.00
		200	7.92	0.14	27.42	1.45	0.60	9.60
		400	5.35	0.00	23.61	1.61	0.45	18.44
		600	5.81	0.10	35.99	1.06	0.38	10.74
		800	4.26	0.13	35.67	1.07	0.36	11.95
13/01/2011	#21 (E151)	20	44.75	1.54	114.13	0.72	1.38	2.58
		35	39.99	1.82	73.37	0.77	0.94	2.29
	53.75°S, 38.98°W	50	48.57	2.03	94.66	1.24	1.36	1.91
		75	25.63	0.91	68.56	0.98	1.17	-
		100	64.06	1.91	114.03	2.33	1.32	1.51
		150	73.04	1.59	62.83	7.70	1.28	12.20

Table 2: SAPS samples: The particulate Fe (PFe), Mn (PMn), and Al (PAl) concentrations in the top 150 m of the water column at the 14 sites visited during JR247. The particulate fraction, P, is the sum of leachable particulate (LP) and refractory particulate (RP). Because of low concentrations, the leachable particulate fraction is indicated in percent of the P fraction. Additional information covers sampling date, site (station) ID, event number, latitude and longitude, and water column depth. (Depths marked by * indicate that the polycarbonate filter was corrupted after retrieving the SAPS)

Date	Site ID	Depth	Particulate (nmol L^{-1})			Leach. Part. (% of P)		
	Lat. & Lon.	(m)	PFe	PMn	PAl	LPFe	LPMn	LPAl
25/12/2010	#1/2 (E22)	20	5.17	0.08	4.82	0.37	2.39	1.65
	53.70°S, 38.21°W	50*	9.12	0.14	7.91	0.27	2.61	1.47
	(322 m)	150*	76.61	1.09	66.91	6.26	2.74	4.65
26/12/2010	#3 (E31)	20	6.62	0.09	6.64	0.02	3.30	0.79
	53.85°S, 39.14°W	50	267.48	3.85	162.59	1.48	0.79	0.65
	(287 m)	150	4.36	0.06	4.26	0.07	1.55	1.93
31/12/2010	#4/5 (E72)	20	8.52	0.12	7.99	0.51	1.68	2.62
	53.49°S, 37.71°W	50	15.15	0.23	12.96	0.56	2.44	2.74
	(1917 m)	150	2.33	0.03	2.15	0.65	1.78	2.42
02/01/2011	#6 (E80)	20	85.74	1.11	59.05	1.60	2.28	4.50
	53.99°S, 36.37°W	50	17.76	0.24	8.87	-	-	-
	(208 m)	150	137.39	2.02	98.54	3.46	0.91	2.81
03/01/2011	#7/8 (E88)	20	1.95	0.02	0.87	0.13	2.97	4.99
	54.10°S, 35.46°W	50	1.67	0.02	0.92	0.08	4.35	4.24
	(330 m)	150	1.23	0.02	0.71	0.19	2.11	5.13
04/01/2011	#9/10 (E96)	20	20.91	0.08	15.74	0.56	5.01	3.24
	54.26°S, 35.35°W	50	19.16	0.27	15.58	0.45	1.22	2.51
	(263 m)	150	54.06	0.77	48.10	1.08	1.65	2.08
05/01/2011	#11/12 (E100)	20*	1.49	0.01	0.86	0.18	4.42	2.92
	54.62°S, 34.81°W	50	0.87	0.01	0.60	0.27	6.63	4.20
	(747 m)	150	1.76	0.03	1.08	0.37	4.38	3.33
06/01/2011	#13 (E106)	20	2.75	0.03	1.78	0.63	3.13	4.29
	54.53°S, 35.27°W	50	4.11	0.05	3.07	0.44	2.04	2.76
	(133 m)	100	10.28	0.15	7.62	0.46	1.70	2.54
07/01/2011	#14 (E114)	20	2.80	0.04	1.84	0.07	1.58	3.29
	54.56°S, 35.59°W	50	1.41	0.02	0.97	0.10	2.57	3.92
	(263 m)	150	31.34	0.46	26.92	0.72	1.57	2.28
08/01/2011	#15/16 (E120)	20	24.54	0.37	22.91	0.85	3.95	1.88
	53.62°S, 36.34°W	50	27.72	0.40	23.23	0.43	3.65	1.36
	(852 m)	150	4.74	0.07	3.94	0.90	4.31	1.06

10/01/2011	#17 (E134)	20	10.43	0.14	8.09	0.34	1.66	2.41
	53.90°S, 36.57°W	50	43.04	0.60	38.79	1.34	1.07	1.67
	(209 m)	150	207.48	3.10	194.88	1.72	0.82	1.50
11/01/2011	#18 (E139)	20	95.52	1.32	88.39	1.39	1.82	1.93
	54.10°S, 36.25°W	50	37.43	0.52	35.33	1.16	1.29	1.85
	(276 m)	150	28.00	0.41	23.60	1.26	2.35	2.27
12/01/2011	#19/20 (E142)	20	97.60	1.52	97.10	0.16	1.66	0.33
	53.54°S, 38.11°W	50	90.96	1.42	92.89	0.39	1.98	0.80
	(1741 m)	150	7.41	0.12	6.37	0.74	8.25	2.75
13/01/2011	#21 (E152)	20	50.75	0.85	52.78	0.06	2.99	0.12
	53.75°S, 38.98°W	50	59.59	0.93	59.98	0.05	2.15	0.09
	(269 m)	150	153.48	2.34	89.63	3.14	1.10	2.94

Table 3: Sediment core samples: Particulate iron (SFe), aluminum (SAl), and manganese (SMn) concentrations in shelf sediments collected during JC055 in January and February 2011. Pore water data retrieved additionally from these three cores are listed for Fe (Fe_{PW}) and Mn (Mn_{PW}). Additional information are event number (MC…), latitude + longitude, and water column depth.

Station ID Lat. & Lon.	Depth (cm)	SFe (mol kg-1)	SAl (mol kg-1)	SMn (mmol kg-1)	Fe_{PW} (µmol kg-1)	Mn_{PW} (µmol kg-1)
#S1 (MC33)	0.5	0.58	1.77	11.56	3.01	2.29
54.16°S, 37.98°W	1.5	0.61	1.74	11.52	17.47	0.84
(257 m)	2.5	0.59	1.77	11.78	110.90	0.28
	3.5	0.6	1.86	12.05	106.24	0.53
	4.5	0.58	1.72	11.82	94.09	0.34
	5.5	0.59	1.86	12.04	82.79	0.27
	9	0.56	1.72	11.19	32.98	0.00
	15	0.55	1.74	11.15	2.44	0.06
	25	0.53	1.6	10.81	0.80	0.16
#S2 (MC34)	0.5	0.64	1.77	11.42	1.53	0.87
54.16°S, 37.94°W	1.5	0.6	1.79	11.73	/	/
(247 m)	2.5	0.58	1.76	11.81	0.97	0.24
	6.5	0.59	1.83	12.23	11.19	0.26
	10.5	0.58	1.8	11.78	14.28	0.25
	14.5	0.54	1.6	10.83	3.59	0.33
	16.5	0.56	1.72	11.22	2.27	0.31
#S3 (MC35)	0.5	0.61	1.67	11.42	1.46	0.43
54.15°S, 37.97°W	1.5	0.59	1.76	11.7	28.94	0.35
(254 m)	2.5	0.58	1.76	11.7	91.52	0.37
	3.5	0.59	1.81	12.03	40.16	0.44
	5.5	0.57	1.78	11.58	49.37	0.56
	8.5	0.59	1.82	11.65	67.92	0.52
	17	0.54	1.69	10.8	3.87	0.34
	19	0.55	1.67	10.86	1.82	0.12
	25	0.55	1.77	11.19	2.73	0.36
	29	0.56	1.79	11.19	5.64	0.16

Table 4: Krill faecal pellets: Particulate (P) and leachable particulate (LP) concentrations for Fe, Mn, and Al determined for the 27 individual krill faecal pellet samples collected during 9 krill incubation experiments on-board RRS *James Clark Ross* (JR247). The particulate fraction, P, is the sum of leachable particulate (LP) and refractory particulate (RP). Because of low concentrations, the leachable particulate fraction is indicated in percent of the P fraction.

# Sample	pellet weight (mg)	PFe ($\mu g\ mg^{-1}$)	PAl ($\mu g\ mg^{-1}$)	PMn ($ng\ mg^{-1}$)	LPFe (%)	LPAl (%)	LPMn (%)
1	4.87	0.88	1.06	12.5	6.33	8.83	13.24
2	2.18	1.33	1.68	16.7	3.02	8.81	8.22
3	4.26	1.07	1.90	17.8	5.37	3.27	11.81
4	1.91	5.19	5.53	76.1	2.15	1.95	5.68
5	1.41	2.70	2.84	39.1	2.46	1.59	3.54
7	7.80	67.1	64.2	998.3	2.93	2.21	3.25
8	0.99	2.71	2.42	35.0	3.76	4.59	5.99
10	1.48	6.42	4.89	71.6	0.29	4.83	0.91
13	2.79	4.13	3.11	50.3	0.36	5.07	1.53
15	0.77	37.3	38.1	531.1	2.03	2.80	6.21
16	1.21	6.35	6.22	81.2	1.24	7.47	3.13
18	12.27	40.0	36.6	582.5	3.95	2.07	4.29
19	2.19	11.2	9.49	146.9	0.15	2.03	1.07
22	2.43	48.1	49.7	721.5	0.81	2.32	0.98
40	3.35	22.8	22.0	337.4	5.51	3.21	5.50
41	8.55	6.91	7.14	103.1	1.11	1.88	4.31
42	3.5	25.7	24.8	376.2	5.09	2.98	5.29
45	0.40	3.96	4.43	43.3	1.27	13.90	1.46
47	7.65	3.63	3.92	52.7	0.34	0.68	3.65
48	0.63	3.06	3.21	34.1	0.05	4.22	0.76
49	4.42	29.6	28.5	438.4	1.65	2.93	1.95
50	7.46	2.31	2.37	34.6	0.36	0.51	2.78
51	5.18	28.0	27.1	431.3	1.85	2.60	2.01
62	1.20	4.63	4.68	68.0	0.31	1.78	0.47
68	2.25	44.0	40.2	667.4	4.84	1.95	4.77
69	1.66	43.6	44.8	663.7	5.66	2.13	5.46
71	3.47	35.3	36.4	557.7	1.50	1.99	1.76

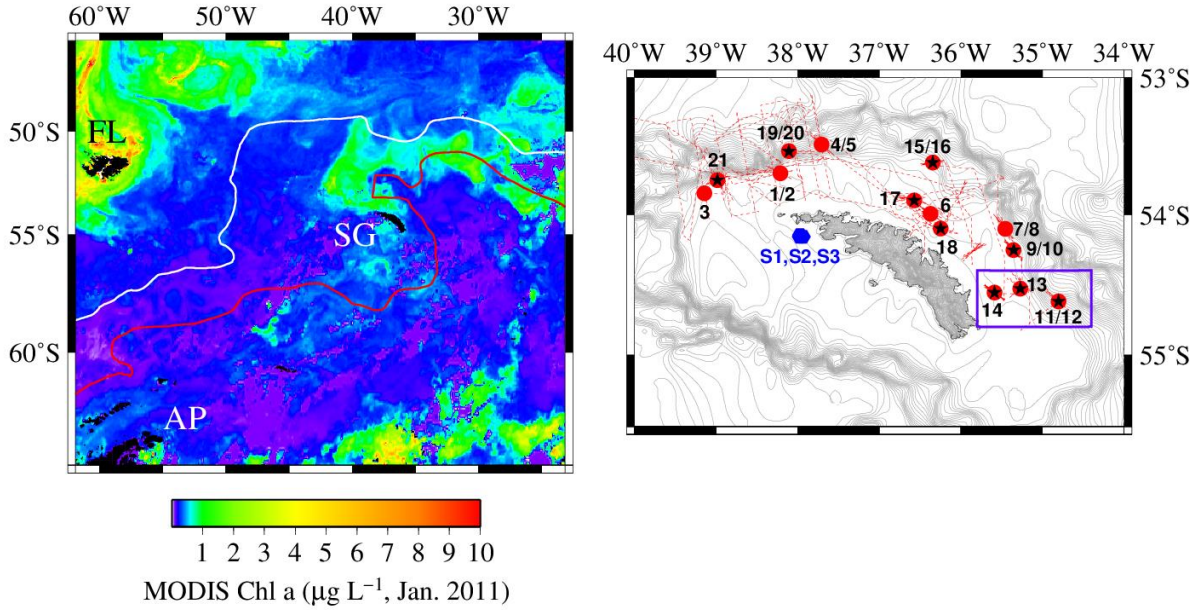

Figure 1: (Left figure) Locations of Falkland Islands (FL), South Georgia (SG), and Antarctic Peninsula (AP) in the Atlantic sector of the Southern Ocean. South Georgia is located between the Antarctic Polar Front (PF, white line) and the Subantarctic Circumpolar Current Front (SACCF, red line). The colour bar represents the Chlorophyll a (Chl a) content recorded by the MODIS satellite in January 2011. (Right figure) The region around SG and the **OTE** (black stars) and **SAPS** sampling sites (red points) visited during JR247. The red dashed line illustrates the cruise track of JR247. The three sediment sampling sites S1, S2, and S3 visited during JC055 are shown by blue hexagons. The purple box indicates the W-E transect from shelf site #14 via site #13 to the shelf edge site #11/12. The ocean bathymetry of the region was plotted using the GEBCO bathymetric data set. The shelf of South Georgia is between 100 and 250 m deep and extends about 30 to 100 km (shelf edge indicated by high density of isobaths).

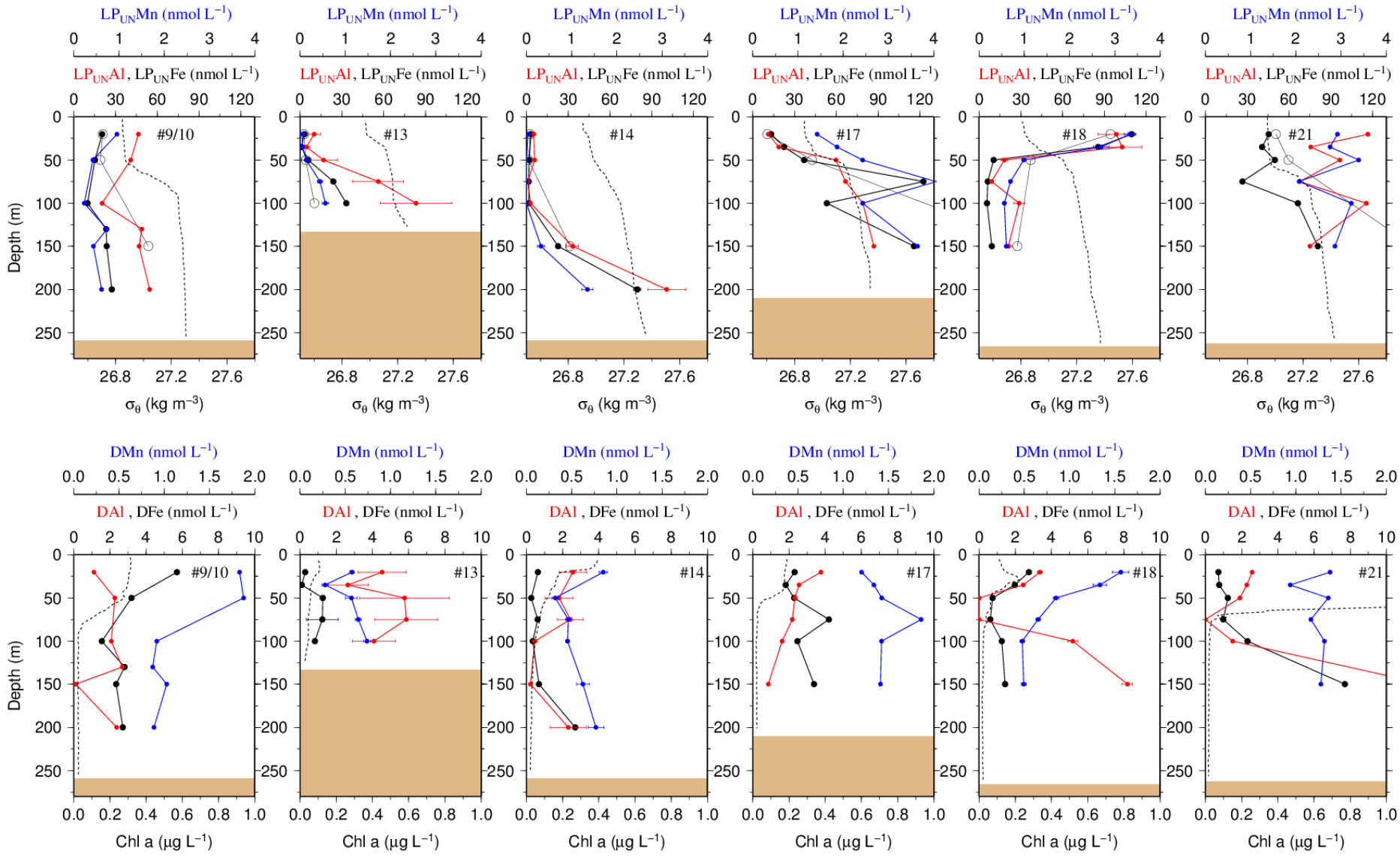
LPUNMn (nmol L−1)
LPUNAl, LPUNFe (nmol L−1)
#9/10
#13
#14
#17
#18
#21
Depth (m)
σθ (kg m−3)
DMn (nmol L−1)
DAl , DFe (nmol L−1)
Chl a (µg L−1)

929

Figure 2: (Upper row) **OTE-seawater samples:** Distribution of leachable particulate iron ($LP_{Un}Fe$ in black), manganese ($LP_{Un}Mn$ in blue), and aluminium ($LP_{Un}Al$ in red) concentrations in the water column of stations located on the island shelf (125 m – 270 m water depth). **SAPS samples:** The particulate Fe (PFe) fraction retrieved by SAPS is illustrated with open black circles and corresponds to the concentration labels of $LP_{Un}Fe$. Concentrations above 120 nmol L^{-1} are listed in Table 1 and 2. Error bars represent the standard deviation of the analysis. Density sigma-theta (σ_θ) in kg m^{-3} is illustrated by the black dashed line. (Lower row) **OTE-seawater samples:** Dissolved iron (DFe), manganese (DMn), and aluminium (DAl) are represented by the same colour code as above. Dashed lines illustrate Chlorophyll a (Chl a) content of the water column recorded by the CTD fluorometer.

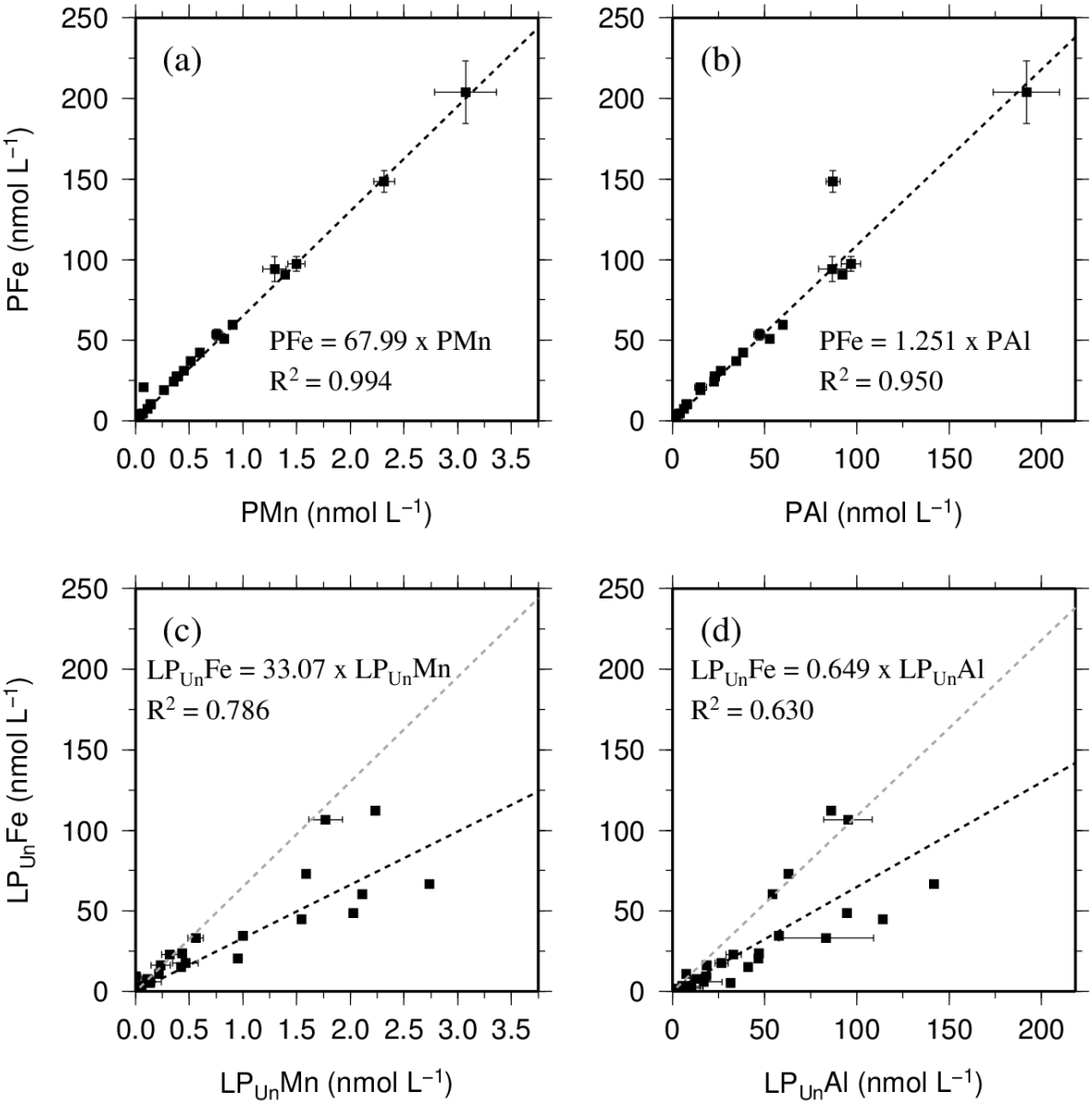

Figure 3: Relationship of the entire data set for the particulate fraction of Fe, Mn, and Al in particulates (P) retrieved using SAPS ((a) and (b)) and the leachable particulate fraction (LP_{UN}) estimated from unfiltered and dissolved seawater samples collected using OTE bottles ((c) and (d)). Error bars represent the standard deviation of the analysis. The linear regression of each relationship is illustrated by a dashed black line, the formula, and the R^2. The grey dashed line in c. and d. represents the linear relationship of particulate trace meals (P) shown in (a) and (b).

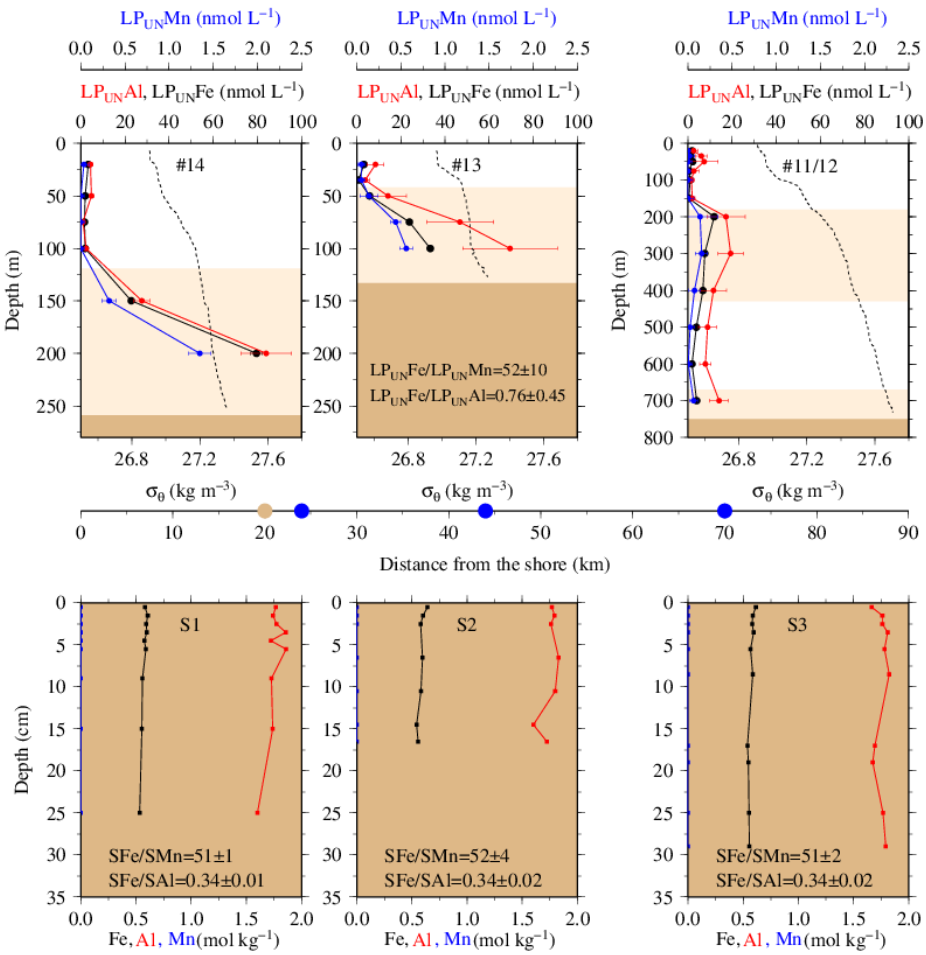

Figure 4: (Upper row) **OTE-seawater samples:** From left to right, concentrations of leachable particulate iron ($LP_{Un}Fe$), aluminium ($LP_{Un}Al$), and manganese ($LP_{Un}Mn$) of unfiltered seawater samples for the two shelf sites #14, #13 and the shelf edge site #11/12 (Note different depth scaling). Error bars represent the standard deviation of the analysis. Water density (sigma-theta (σ_θ)) is shown by the dashed black line. Brown areas represent sediments and pink areas the zone of resuspended sediment particles in the water column. Diagram 14 (left) contains the average $LP_{Un}Fe/LP_{Un}Al$ and $LP_{Un}Fe/LP_{Un}Mn$ ratio of particles in seawater samples collected within the pink layers. (Lower row) **Sediment core samples:** Diagram S1, S2 and, S3 displays the Fe, Mn, and Al content in the three sediment cores. Shown are average SFe/SAl and SFe/SMn ratios (mol/mol) of particles from the surface layer for site S1, S2, and S3. Dots on the distance scaling in the middle represent the distance of each water column station (blue) and sediment core (brown) station to the nearest shore.

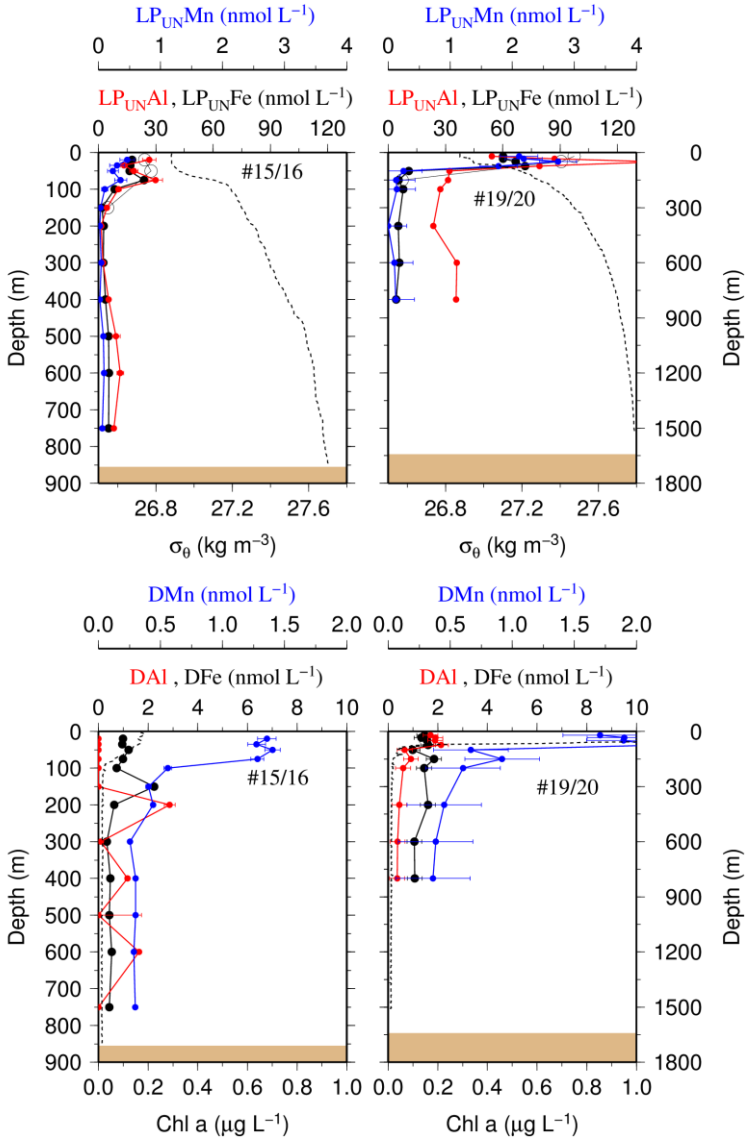

Figure 5: (Upper row) **OTE-seawater samples:** Distribution of leachable particulate manganese ($LP_{Un}Mn$ in blue), iron ($LP_{Un}Fe$ in black), and aluminium ($LP_{Un}Al$ in red) concentrations in the water column of the two other stations located on the island shelf edge (> 700 m water depth). **SAPS samples:** The particulate Fe (PFe) is illustrated by black circles and corresponds to the concentration labels of $LP_{Un}Fe$. Error bars represent the standard deviation of the analysis. Sigma-theta (σ_θ) is illustrated by the black dashed line. (Lower row) **OTE-seawater samples:** Dissolved manganese (DMn), iron (DFe), and aluminium (DAl) are represented by the same colour code as for the upper row. Dashed line illustrates the Chl a content of the water column recorded by the CTD mounted fluorometer.

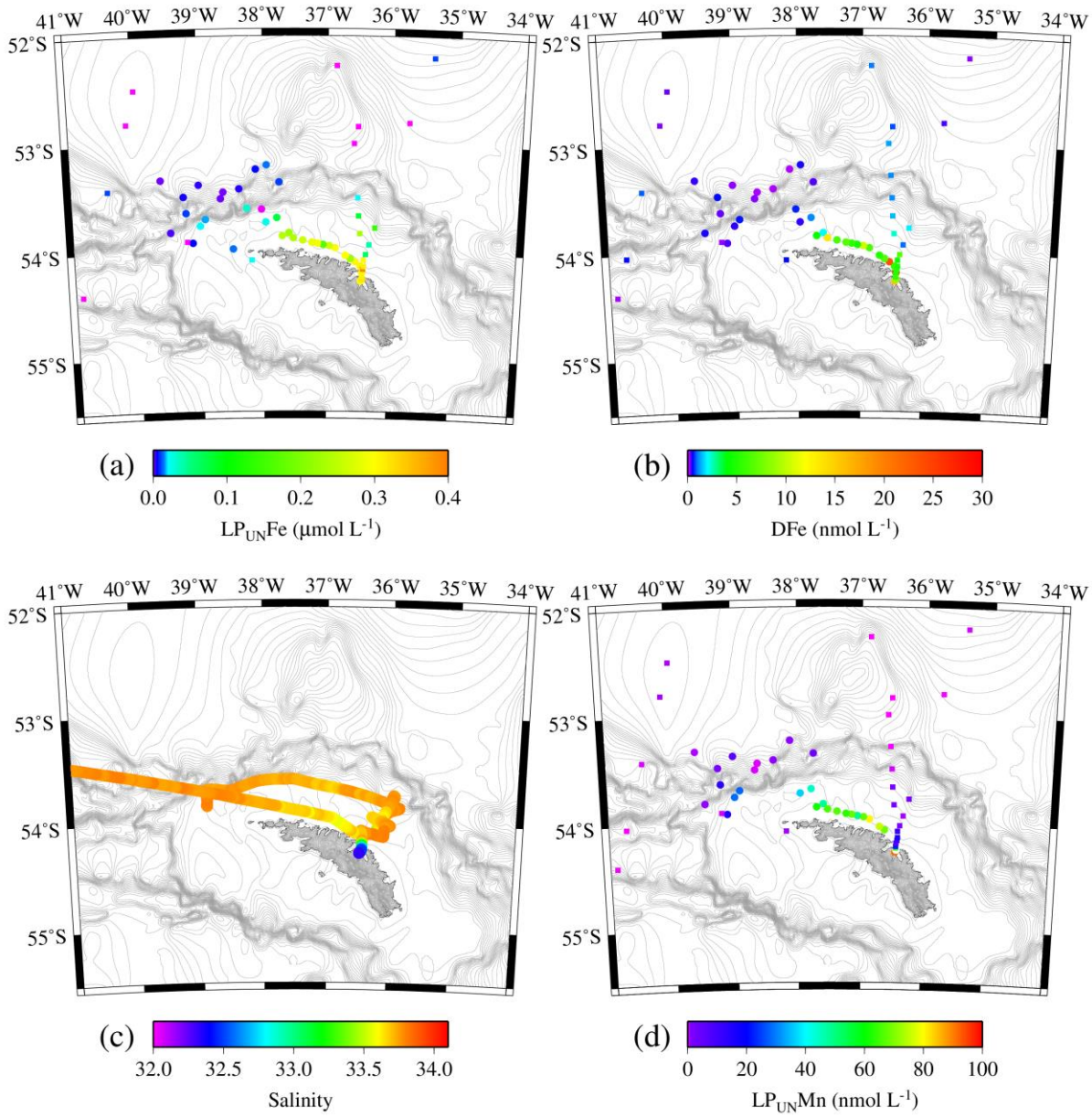

Figure 6: Tow fish-seawater samples: Concentrations of leachable particulate Fe ($LP_{UN}Fe$) of unfiltered seawater samples (a), dissolved Fe (DFe) (b), Salinity (c) and leachable particulate Mn ($LP_{UN}Mn$) in unfiltered seawater samples (d) in surface waters collected during JR247 (circles) and JR274 (squares) around South Georgia. The highest $LP_{UN}Fe$ concentration was recorded in a single sample in Cumberland Bay reaching 2.2 µmol L^{-1}. Because of generally lower concentrations we excluded this data point in panel (a). Isobath are represented by grey lines (GEBCO – Gridded Bathymetry Data).

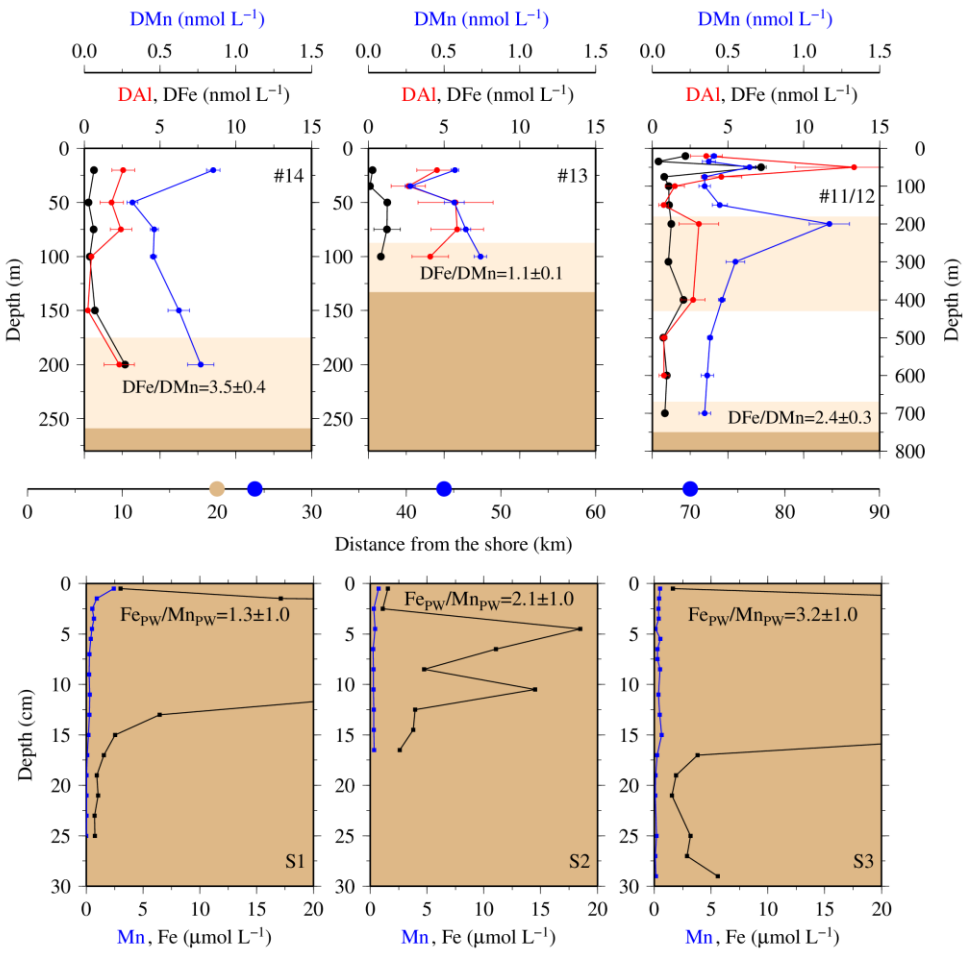

Figure 7: (Upper row) **OTE-seawater samples:** From left to right, concentrations of dissolved iron (DFe), aluminium (DAl), and manganese (DMn) for the two shelf sites (#14, #13) and the shelf edge site (#11/12). Note different depth scaling. Error bars represent the standard deviation of the analysis. Pink areas represent the zone of resuspended sediments in the water column. The DFe/DMn ratios of the seawaters collected within the pink zone is indicated. (Lower row) **Sediment core samples:** Diagram S1, S2 and, S3 displays the Fe (black), and Mn (blue) content in pore waters of the three sediment cores. Values off-axis can be found in Table 3. Shown are average Fe_{PW}/Mn_{PW} ratios (mol/mol) of top surface layer (1 cm) for site S1, S2, and S3. Dots on the distance scaling in the middle represent the distance of each water column station (blue) and sediment core (brown) station to the nearest shore.

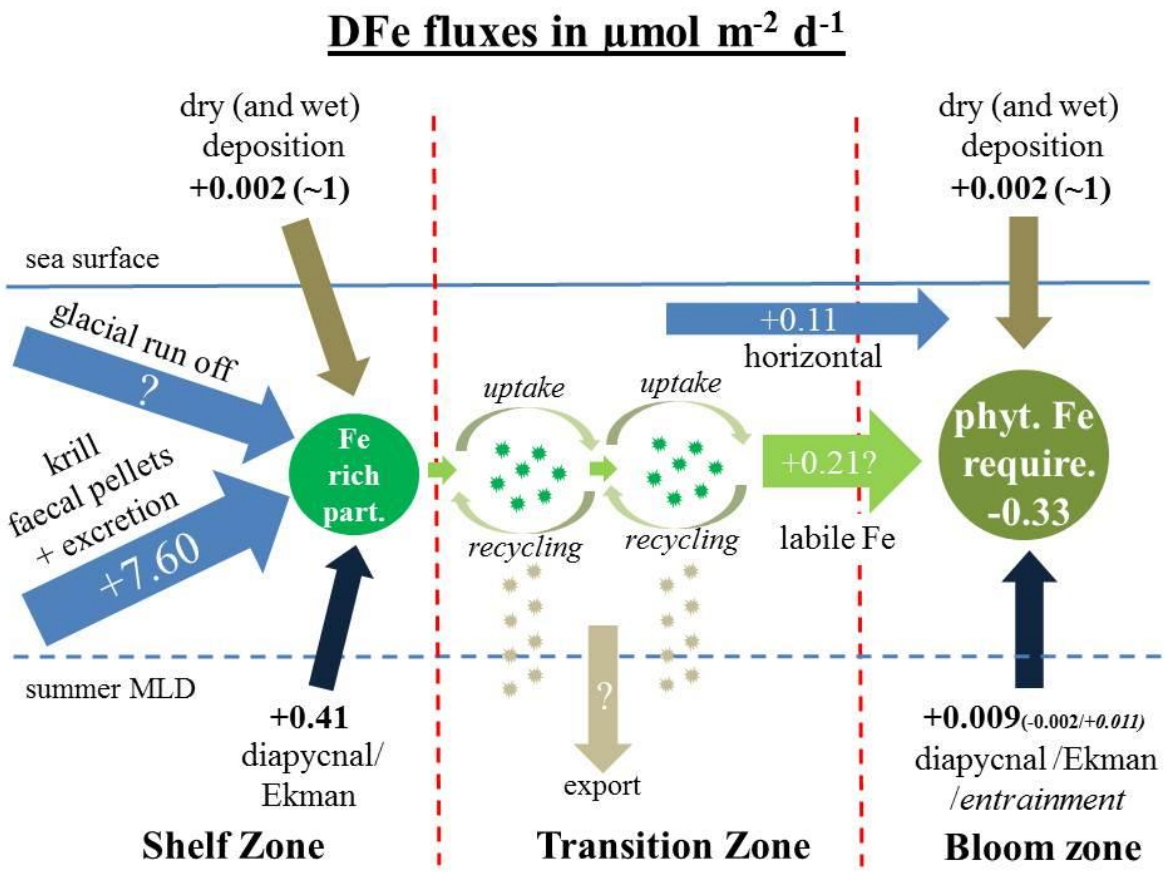

Figure 8: Sketch of DFe fluxes on the shelf, in the transition zone and in the downstream blooming region, separated by the red dashed lines. (left sketch) Describes the dissolved Fe fluxes on the shelf that together generate Fe rich biogenic and lithogenic particles (dark green). These are transferred offshore (light green arrows) following the ACC to open ocean sites (sketch in the middle). Iron enriched particles (dark green) in the transition zone are recycled and supplement DFe requirements of the phytoplankton community in the transition zone. During each cycle of recycling and uptake an unknown Fe fraction is lost by vertical export. (right sketch) Describes the dissolved Fe fluxes in the blooming zone.